# THE EFFECTS OF RANGE AND HEIGHT

# ON

# RADAR MEASUREMENTS OF STORMS

by

NANCY THERESE LUKITSH

SUBMITTED IN PARTIAL FULFILLMENT
OF THE REQUIREMENTS FOR THE
DEGREE OF

BACHELOR OF SCIENCE

at the

MASSACHUSETTS INSTITUTE OF TECHNOLOGY

May, 1978

Signature of Author.....
Department of
Earth and Planetary Sciences
May 18, 1978

Certified by.....
Thesis Supervisor

Accepted by.....
Chairman, Undergraduate Studies

ABSTRACT

THE EFFECTS OF RANGE AND HEIGHT
ON RADAR MEASUREMENTS OF STORMS

by Nancy Therese Lukitsh

Submitted to the Department of Earth and Planetary Sciences
on May 18, 1978, in partial fulfillment of the requirements
for the degree of Bachelor of Science.

Traditional methods of radar data collection have two major disadvantages: (1) data displays taken at constant elevation angles reveal little about storm structure; and (2) by the nature of the radar, there are certain range dependent effects including attenuation, resolution and minimum detectable signal, which must be taken into account when analysis is done. This thesis represents an effort to address these difficulties by means of a constant-height study of the intensity distribution in four New England storms at different heights and different ranges. Through this analysis, an attempt is made to investigate the nature, influence and degree of variability of the effects mentioned above.

The possible range effects can be predicted to some extent. Attenuation by atmospheric gases can be computed from the temperature, pressure and vapor content along the path of the ray. The effect of the minimum detectable signal variation is predicted using two different models which are dependent on storm type. The resolution effect can be hypothesized based on the known results of beam broadening. These predictions and hypotheses are then tested utilizing actual storm data. It is concluded that the various effects are of sufficient magnitude to be significant, especially in statistical studies using data from a large number of ranges and a variety of heights.

Thesis Supervisor: Pauline M. Austin
Position: Senior Research Associate
Department of Meteorology

Acknowledgements

This thesis would not have been possible without the support and guidance of my thesis advisor, Dr. Pauline M. Austin. Her interest and enthusiasm were a constant source of encouragement.

Special thanks are due Judson E. Stailey for countless hours of patient tutoring in the intricacies of computer programming. Additional lessons in this area were provided by Frank Marks, Jr., Craig Goldman and Alan Siggia; they too have my gratitude.

Also on the 18th floor, Spiros Geotis was a ready source of information on a wide variety of items having to do with radar data.

Carol and Joanne Lukitsh, Mr. and Mrs. Robert Lukitsh, Dorothy Klepacz and Regina Wiedenski maintained support and interest in this project over the year and a half that it was in progress. This support and interest played a large part in its completion.

This thesis is dedicated to my parents, with love.

Table of Contents

## Introduction

Since the first discovery of weather "clutter" on radar scopes used in World War II, radars have become necessary observational tools in studies of precipitation growth and storm development. A good deal of information about storm structure can be discerned from radar scope displays of precipitation echoes. Among the features which have been noted are tendencies for heavier rain to occur in large mesoscale areas of about $10^3$ square kilometers, and the tendency for these areas to be organized into rainbands or lines of showers. However, information such as statistics on the nature and degree of organization in different storms and the characteristic sizes and spacing of precipitation areas are very difficult and tedious to extract from sequential scope display photographs. Now though, with the availability of digital recording and processing, we are in a position to seek and analyze such statistics.

Radar data are collected as a function of range along a ray which emanates from the radar site in the direction determined by the azimuth and elevation angles of the antenna. The most effective and convenient mode for obtaining three-dimensional coverage of storms is to scan the antenna $360^\circ$ in azimuth, through a series of elevation angles, thus sweeping out a set of conical surfaces in space. The drawbacks of the use of this system for meteorological analysis are twofold: (1) the three-dimensional nature of storm structure is such that, while horizontal and

vertical cuts reveal certain patterns, a constant elevation angle sweep reveals little in the way of structure; and (2) by the nature of the radar, there are certain range dependent effects including attenuation, resolution and minimum detectable signal, which must be taken into account when analysis is done. Thus in analyzing a storm from radar observations, one must be able to distinguish between effects which reflect changes in storm structure or intensity and those which are instrumental or range dependent.

This study endeavors to cope with both of these problems through thorough analysis of data recorded during four different New England storms. In these storms, precipitation patterns differ considerably thus it is undesirable to combine storms to get a larger data sample. An attempt is made to observe the range effects by considering how measured intensity distributions vary with height and range. In order to observe these range effects, the radar field is divided into eight concentric rings with a radius increment of thirty-two kilometers. Since precipitation patterns show considerable horizontal variability over the area viewed by the radar, not all differences observed in intensity distributions can be attributed to instrumental or range effects. However, it is hoped that the natural storm variations which exist will not completely mask any significant range effects.

Some range effects are predictable. For example, the signal varies as $1/r^2$, where r is equal to the range. However, normalization is included for this known experimental variation. But there are other effects about which less is known. These include attenuation of microwave radiation by atmospheric gases. This

can be computed from the temperature, pressure and vapor content along the path of the ray. Such computations are discussed in Chapter 2.

Probably the most important range effect though, is that the minimum detectable value of intensity increases with range. The expected effect of this factor is illustrated by the models in Figures 1 and 2.

In this study, we are primarily concerned with spatial intensity distributions which are represented by the fraction of data points which contain precipitation of different intensities. The two figures represent two different storm types which are believed to be realistic. The heavy outer line represents the actual intensity distribution in any range ring. The light lines represent the intensity distribution, deduced from radar measurements in the various range rings. Dashed lines indicate the minimum detectable intensity for the range ring boundaries.

In each case, at the intensity representing the minimum detectable value for the outer boundary of a given range ring, the observed frequency begins to drop away from the actual one, reaching zero at the minimum detectable value for the inner boundary. This effect is explained by the definition of the minimum detectable signal as the smallest signal which can be detected above the noise level. That is, the large number of points which constitute a ring intensity peak serve to screen out that intensity in the more distant rings. The differences between Figures 1 and 2 are due to the fact that most storms apparently

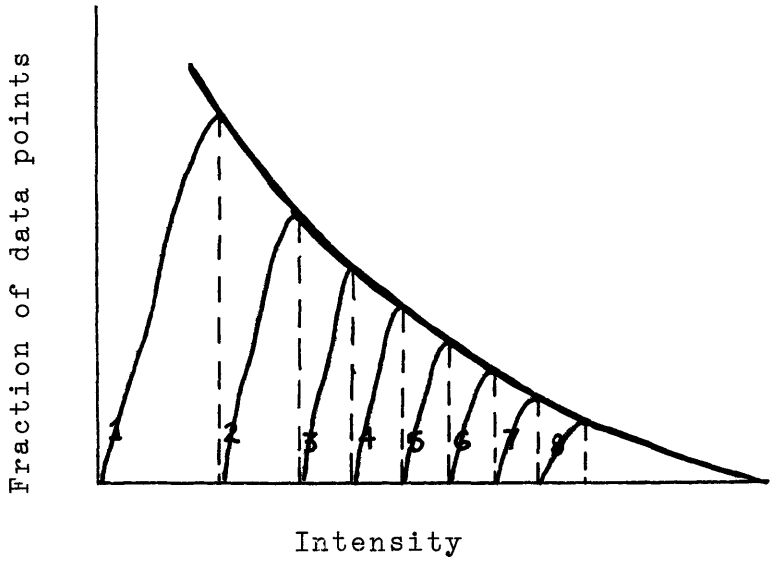


Figure 1. The sloping model.

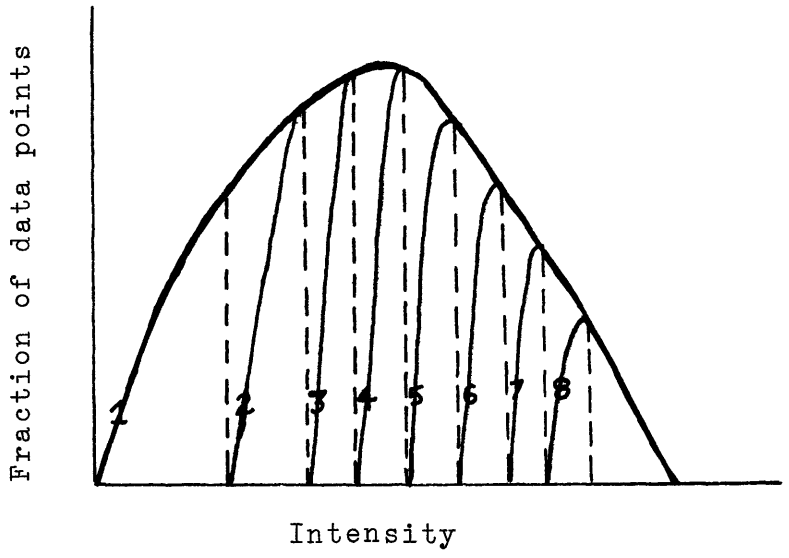


Figure 2. The peaked model.

have relatively large areas of light rain, so that Figure 1 is a more typical distribution. Figure 2 represents a storm which has a preferred rainfall rate at a somewhat higher intensity.

A third range effect may result from the spreading of the radar beam with range. This has the effect of increasing the volume of atmosphere sampled, thus smearing individual values at larger ranges. For example, small intense showers might be averaged over a larger area so that peak values would be lower at farther ranges than at closer ones.

In order to study meteorological effects, the data were analyzed not at a constant elevation angle, but at a constant height. This was because storm reflectivities change significantly with height as falling hydrometeors grow and melt. Therefore, range effects cannot be studied as such unless the various range rings are from the same height in the atmosphere. However, this constant-height analysis had drawbacks which included the horizon effect at low levels. This effect is a result of the earth's curvature away from the radar beam and can cause a lack of data at low levels and long ranges.

However, with the knowledge of these difficulties of both a meteorological and instrumental nature, there still exists the possibility of significant analysis of various types of New England rain storms. This study will endeavor to provide information about the magnitude of range biases in different types of storms. Such information should make it possible for studies of storm structure and behavior to be based on data from the entire area covered by the radar without being distorted by range effects.

## Methods of Data Gathering and Analysis

### The data.

Data for this study were recorded in the Weather Radar Laboratory at the Massachusetts Institute of Technology. Measurements were made using the WR66 and WR73 radars, the characteristics of which are summarized in Table 1.

Table 1. Characteristics of the WR66 and WR73 radars.

| Parameter | WR66 | WR73 |
|---|---|---|
| Wavelength ($\lambda$)(cm.) | 10.5 | 5.5 |
| Nominal transmitted power (kw.) | 600. | 250. |
| Antenna diameter (ft.) | 18. | 8. |
| Antenna gain (dB) | 41.9 | 38.8 |
| Beam width (degrees) | 1.35 | 1.4 |
| Pulse length ($\mu$ sec.) | 1. | 2. |
| Frequency (MHz.) | 2850. | 5550. |

The WR73 radar is run in conjunction with a TI 980A minicomputer for recording data and is known as the GATE system. Mean echo intensities are recorded in engineering units for polar coordinate bins in three dimensions. Resolution in intensity is 0.4 dB. In range, resolution is variable with 512 bins covering a total range of 256 km. The other system is designated HRP and uses the WR66 radar with a PDP-8 minicomputer to record maps on dectapes. This system records in 100 range bins with a resolution of $\frac{1}{2}$, 1 or 2 nautical miles. Most New England data is recorded on the HRP while further analysis of that data is done on the TI 980A. But first, the dectapes must be copied onto 9 track magnetic tape and transposed to the format used for recording with the GATE system.

In both systems, data are recorded for every degree in

azimuth and at a series of eleven elevation angles between 0 and 30 degrees (See Table 2). The recorded intensities are range

Table 2. Elevation Angles

| Tilt Number | Nominal Elevation Angle (degrees) |
|---|---|
| 1 | .5 |
| 2 | 1 |
| 3 | 2 |
| 4 | 3 |
| 5 | 4 |
| 6 | 6 |
| 7 | 8 |
| 8 | 10 |
| 9 | 15 |
| 10 | 20 |
| 11 | 30 |

normalized and can be converted directly to equivalent radar reflectivity factors or equivalent rainfall rates.

The radar reflectivity factor of a volume of atmosphere containing precipitation depends on the number and size of the hydrometeors contained within that volume. This factor is denoted by Z and is equal to the sum of the sixth power of the diameters (or equivalent diameters for non-spherical particles) of the hydrometeors in a unit volume. The factor has units of $mm^6 m^{-3}$ which are more commonly expressed in logarithmic units of dBZ, that is $10\log_{10}Z$. For example, 40 dBZ corresponds to $10^4$ $mm^6 m^{-3}$. The effective or equivalent Z value, $Z_e$, is a value which is deduced from radar measurements rather than from direct observations of the hydrometeors.

Distribution of reflectivity at different heights and ranges.

For this study, a program was devised to assimilate data recorded at a specific height rather than data recorded at a given elevation angle. The program accomplishes this goal by computing the intensity distributions within selected range and

height intervals. These intervals can be varied, but for this study thirty-two kilometer range intervals and two kilometer height intervals were used. Storm by storm distributions were compiled for nominal heights of two, four and six kilometers. The results are presented in a table which indicates the total number of data points per ring, sorted according to the reflectivity values which each point possesses (See Appendix I). To facilitate the handling of such large amounts of data, the intensity distribution is represented using reflectivity factor intervals of 2 dBZ.

A result of this method of analysis is that at short ranges, rays from more than one elevation angle may fall within the height interval being analyzed while at longer ranges there may be fewer data points available. This causes an uneven distribution of points into the different range rings, thus posing some problems in comparing the results at different ranges. The extent of this discrepancy can most clearly be seen in Appendix II which lists the number of points for each range ring and height. To overcome this difficulty a fractional table was compiled which presents the fraction of data points per ring which fall in the given reflectivity interval (See Appendix I). This table then provides a good comparison of how the reflectivity values vary from one range ring to the other as well as how these values vary within the same range ring for different heights and/or times.

A further basis of comparison is provided by a summary table (See Appendix III). This table provides, for each nominal height under study, a listing of the total number of points in each range ring and within each reflectivity interval for all of the map times under consideration in a given storm. There is a need for this because, at any one time, an important mesoscale feature may be located almost entirely within a single range ring. Thus samples in the different rings are not representative of the overall intensity distribution of the storm. When a number of maps which span a period of hours are combined, the important mesoscale features are recorded in all the range rings as they move across the area viewed by the radar. The result is a more representative storm distribution.

Initially, the problem of constant-height analysis was dealt with by considering each kilometer bin along the line of constant height and determining which angle of elevation passed closest to that particular bin. From Figure 3, which shows the height of the beam center for different ranges and elevation angles, it can be seen that, at 2 km., in range ring 2, for example, covering the distance from 32 km. to 64 km., values for the first 11 points would be those recorded at an elevation angle of $3^{\circ}$ and those for the remaining 21 points would come from the $2^{\circ}$ elevation. After the correct angle was determined, the reflectivity value for that height, kilometer and elevation angle was recorded in the range ring in which it fell. The printout format was the same, a chart of the number of points of specific reflectivity intervals in each range ring.

Figure 3. Beam center height for different ranges and elevation angles.

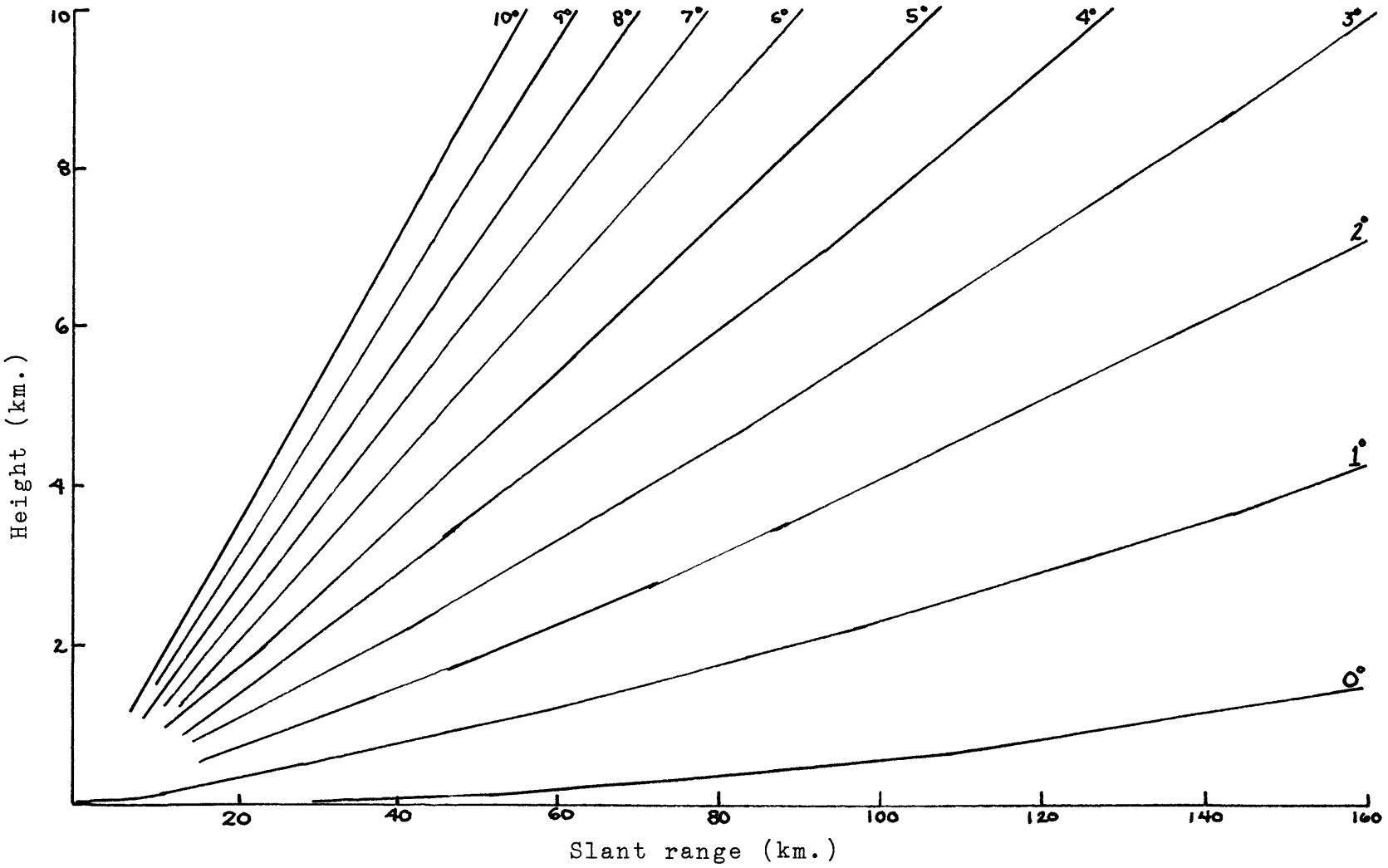

This earlier technique had the advantage of having the same number of points in each range ring, but it also had a serious disadvantage. Specifically, although each range bin was assigned a reflectivity value drawn from the nearest elevation angle, in the farther range rings, the closest angle was often one to two kilometers away. The result was that this method presented spurious results in the outer rings and so was replaced by the previously described "interval" method of analysis.

Effects of atmospheric attenuation.

A final important feature of the "interval" program is its ability to take the effects of attenuation into account. Attenuation is defined by Battan (1973) as the "loss of power as the transmitted pulse passes from the antenna to the target or as the reflected power returns to the antenna". It can be caused by atmospheric gases, clouds, and precipitation and is the result of two effects: (1) absorption, and (2) scattering of power out of the beam.

For this study, the effect of attenuation by clouds has been ignored. Work done by Gunn and East (1954) indicates that for radar with wavelengths of 10.5 and 5.5 cm., the one-way attenuation coefficients in dB $km^{-1}$ per g $m^{-3}$ are of the order of magnitude of $10^{-2}$ for water clouds and $10^{-4}$ for ice clouds. But since clouds with water content of a g $m^{-3}$ or more generally have horizontal extents of only a few kilometers, these quantities are small enough to be ignored for this study.

Attenuation due to rainfall was also not considered,

although research has been done in the Weather Radar Laboratory to allow for it (Geotis, 1975). However, at a wavelength of 10.5 cm., attenuation due to rainfall is not significant and at the 5.5 cm. wavelength, attenuation only becomes important for very heavy thunderstorms. It was therefore not included in this study.

The attenuation which was calculated was that caused by absorption by atmospheric gases, specifically, water vapor and oxygen. Because the individual molecules behave like dipoles, each gas absorbs energy. Water vapor has a permanent electric dipole moment, while oxygen has a permanent magnetic dipole moment. As the incident electromagnetic wave passes over these molecules, it reacts with them causing oscillation and rotation in a variety of ways. According to quantum theory, each individual vibrational state is associated with a particular energy level. While at the new energy level, a certain amount of energy is needed to maintain the molecules, and this is given by hf, where h is Planck's constant and f is frequency. Therefore, it can be said that the incident wave delivers to the gas molecules discrete parcels of energy (hf) during the transition from the lower- to the higher-energy level. Although the energy is reradiated when the molecule returns to the lower level, the reradiation is random and this energy does not add to the exciting wave. The result, therefore, is an attenuation of the amplitude of the incident wave.

To calculate the average atmospheric attenuation for the New England storms under consideration, an average sounding for

January and July at latitude 45°N was used (See Tables 3 and 4). Relative humidities given in the tables were converted to vapor densities by the following relations, in which it is assumed that water vapor in the atmosphere behaves as an ideal gas:

$$e = \rho_v R_v T \qquad (1)$$

$$f \cong 100(e/e_s) \qquad (2)$$

$$\rho_v = (e_s f/R_v T) \qquad (3)$$

where e = vapor pressure, $R_v$ = individual gas constant for water vapor ($4.615 \times 10^6$ dynes cm $g^{-1}$ $°K^{-1}$), T = temperature, $\rho_v$ = vapor density, f = relative humidity and $e_s$ = saturation vapor pressure over water.

Table 3. Average January sounding at 45°N latitude.

| Height (km) | Relative Humidity | T (°K) | $e_s$ (dyne/cm$^2$) | $\rho_v$ (g/m$^3$) |
|---|---|---|---|---|
| 0 | .77 | 272.59 | $5.847 \times 10^3$ | 3.58 |
| 1 | .70 | 269.00 | $4.477 \times 10^3$ | 2.52 |
| 2 | .65 | 265.43 | $3.427 \times 10^3$ | 1.82 |
| 3 | .55 | 261.86 | $2.582 \times 10^3$ | 1.18 |
| 4 | .50 | 255.79 | $1.565 \times 10^3$ | .66 |
| 5 | | 249.76 | $.931 \times 10^3$ | |
| 6 | .45 | 243.73 | $.538 \times 10^3$ | .19 |
| 7 | | 237.73 | $.302 \times 10^3$ | |
| 8 | .35 | 231.72 | $.163 \times 10^3$ | .05 |
| 9 | | 225.74 | $.085 \times 10^3$ | |

Table 4. Average July sounding at 45°N latitude.

| Height (km) | Relative Humidity | T (°K) | $e_s$ (dyne/cm$^2$) | $\rho_v$ (g/m$^3$) |
|---|---|---|---|---|
| 0 | .75 | 296.22 | $28.256 \times 10^3$ | 15.50 |
| 1 | .65 | 291.14 | $20.630 \times 10^3$ | 9.98 |
| 2 | .55 | 286.20 | $15.067 \times 10^3$ | 6.27 |
| 3 | .45 | 279.79 | $9.742 \times 10^3$ | 3.40 |
| 4 | .40 | 273.57 | $6.288 \times 10^3$ | 1.99 |
| 5 | | 267.45 | $3.997 \times 10^3$ | |
| 6 | .30 | 261.33 | $2.480 \times 10^3$ | .62 |
| 7 | | 254.81 | $1.450 \times 10^3$ | |
| 8 | .30 | 248.28 | $.814 \times 10^3$ | .21 |
| 9 | | 241.77 | $.445 \times 10^3$ | |
| 10 | .30 | 235.27 | $.235 \times 10^3$ | .07 |

Both tables from U.S. Standard Atmosphere Supplements, 1966, $e_s$ from Smithsonian Tables.

With this information available, findings of Gunn and East (1954) listed in Table 5 on water vapor attenuation were then utilized to calculate that attenuation at discrete one kilometer intervals. As the attenuation was only slightly dependent on temperature, the sounding temperatures were rounded to the nearest values given by Gunn and East, i.e. -40, -20, 0 or 20 $^{o}$C. In addition, due to the lack of availability of more detailed research in the field, the values for a wavelength of 10 cm. had to be used when the wavelength was actually 10.5 cm. and the values for a wavelength of 5.7 cm. had to be used when the wavelength was 5.5 cm.

Table 5. Water-vapor attenuation (one-way) in decibels per kilometer.

| Temperature ($^{o}$C) | 10 cm wavelength | 5.7 cm wavelength |
|---|---|---|
| 20 | $0.07 \times 10^{-3}$ PW | $0.24 \times 10^{-3}$ PW |
| 0 | $0.08 \times 10^{-3}$ PW | $0.27 \times 10^{-3}$ PW |
| -20 | $0.09 \times 10^{-3}$ PW | $0.30 \times 10^{-3}$ PW |
| -40 | $0.10 \times 10^{-3}$ PW | $0.34 \times 10^{-3}$ PW |

P = pressure in atmospheres
W = water-vapor content, in grams per cubic meter
(from Gunn and East, 1954)

The values given by Gunn and East (1954) were also used to determine attenuation due to oxygen in the atmosphere. Although two different data profiles are presented in their work (based on varying assumptions about the bandwidths of the oxygen absorption lines), this study is based on the higher one (Figure 4 (b)) which has been most commonly used in the literature. The extent of this type of attenuation is dependent on radar wavelength, temperature and pressure in the manner shown in Table 6.

Erratum

page 14, lines 26-27 read "based on the higher one (Figure 4(b))". These lines should read "based on the lower one (Figure 4(a))".

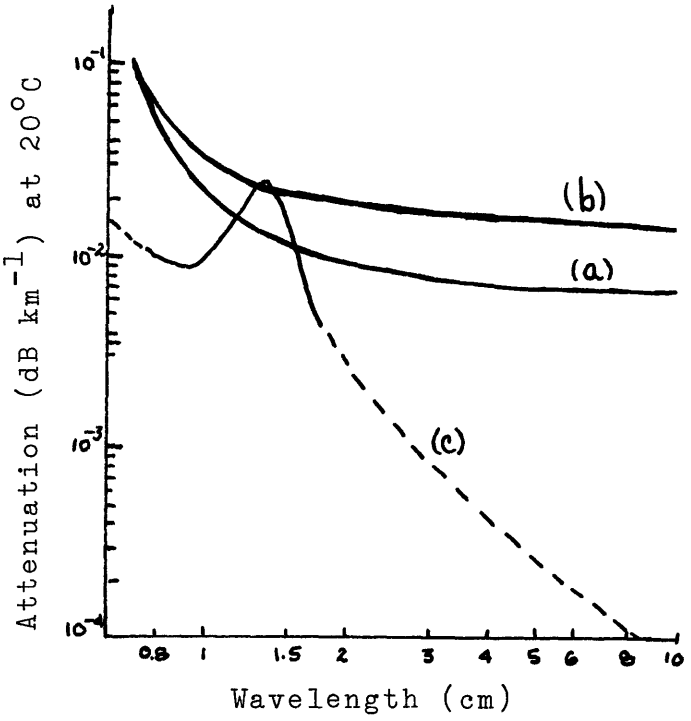


Figure 4. Atmospheric attenuation versus wavelength. (from Gunn and East, 1954)

Table 6. Pressure and temperature correction for oxygen attenuation for wavelengths between 0.7 and 10.0 cm.

| Temperature (°C) | Factor |
|---|---|
| 20 | $1.00P^2$ |
| 0 | $1.19P^2$ |
| -20 | $1.45P^2$ |
| -40 | $1.78P^2$ |

P = pressure in atmospheres
(from Gunn and East, 1954)

The results of the attenuation calculations can be seen in Table 7. The January results were applied to the months from October to March, inclusive, while the July results were used for the remaining months.

Table 7a. 10 cm. attenuation at 45°N latitude.

| January | | July | |
|---|---|---|---|
| Height(km) | Attenuation(dB/km) | Height(km) | Attenuation(dB/km) |
| 0 | $1.740 \times 10^{-2}$ | 0 | $1.617 \times 10^{-2}$ |
| 1 | $1.340 \times 10^{-2}$ | 1 | $1.230 \times 10^{-2}$ |
| 2 | $1.030 \times 10^{-2}$ | 2 | $.945 \times 10^{-2}$ |
| 3 | $.970 \times 10^{-2}$ | 3 | $.857 \times 10^{-2}$ |
| 4 | $.738 \times 10^{-2}$ | 4 | $.660 \times 10^{-2}$ |
| 5* | $.582 \times 10^{-2}$ | 5* | $.567 \times 10^{-2}$ |
| 6 | $.425 \times 10^{-2}$ | 6 | $.473 \times 10^{-2}$ |
| 7* | $.360 \times 10^{-2}$ | 7* | $.375 \times 10^{-2}$ |
| 8 | $.294 \times 10^{-2}$ | 8 | $.276 \times 10^{-2}$ |
| | | 10 | $.192 \times 10^{-2}$ |

Table 7b. 5.7 cm. attenuation at 45°N latitude.

| January | | July | |
|---|---|---|---|
| Height(km) | Attenuation(dB/km) | Height(km) | Attenuation(dB/km) |
| 0 | $1.880 \times 10^{-2}$ | 0 | $2.14 \times 10^{-2}$ |
| 1 | $1.430 \times 10^{-2}$ | 1 | $1.54 \times 10^{-2}$ |
| 2 | $1.090 \times 10^{-2}$ | 2 | $1.11 \times 10^{-2}$ |
| 3 | $1.000 \times 10^{-2}$ | 3 | $.947 \times 10^{-2}$ |
| 4 | $.755 \times 10^{-2}$ | 4 | $.707 \times 10^{-2}$ |
| 5* | $.592 \times 10^{-2}$ | 5* | $.593 \times 10^{-2}$ |
| 6 | $.429 \times 10^{-2}$ | 6 | $.479 \times 10^{-2}$ |
| 7* | $.362 \times 10^{-2}$ | 7* | $.380 \times 10^{-2}$ |
| 8 | $.294 \times 10^{-2}$ | 8 | $.280 \times 10^{-2}$ |
| | | 10 | $.192 \times 10^{-2}$ |

*Because information concerning the average relative humidity at 5 and 7 km., 45°N latitude was not listed in the standard atmospheric tables, these figures represent: an average of the values at 4 and 6 km. for the 5 km level and an average of the values at 6 and 8 km. for the 7 km. level.

It is obvious that the difference in attenuation between the wavelengths of 10 cm. and 5.7 cm. is quite small. Therefore, these results were applied to the 10.5 cm. and 5.5 cm. radars in the Weather Radar Laboratory with little fear of discrepancy. In addition, differences in attenuation in the winter and summer soundings are small (about $10^{-3}$ dB/km), so that errors introduced by using only two mean soundings to cover all seasons would be only a few tenths of a decibel for ranges less than 250 km. Although there is a day to day variation in the relative humidity, the attenuation due to oxygen dominates and therefore relative humidity variation would not cause significant differences in the attenuation.

Although the actual calculated attenuation factors are small, when considered over a distance of 200 to 250 km., they can add up to a difference of one to two dBZ. This effect can perhaps best be seen through application to the minimum detectability model discussed in Chapter 1. Figure 5 is a simplified representation of that model. The dotted line indicates the curve which is actually detected by the radar. However, the dark, solid curve is the true curve, unaffected by attenuation. The amount of displacement would depend on the height in the atmosphere and the range at which the data are taken. The purpose of adding in an attenuation factor is to try and boost the detected curve as close as possible to the true curve.

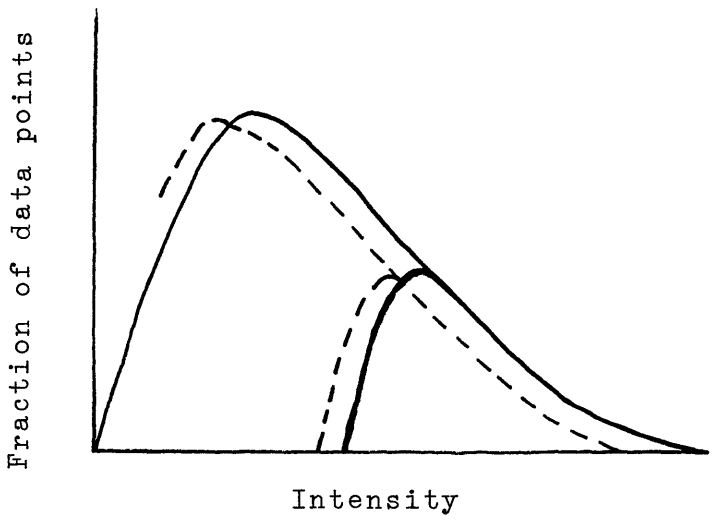


Figure 5. Modified sloping model showing the effects of attenuation.

Expected dependence of minimum detectable signal on range.

Although the exact placement of the individual curves on a graph is storm dependent, it is possible to develop a relationship between the reflecting values which mark the minimum detectable signal for each range ring. This can be done using the basic relation of $P \propto 1/r^2$. In units of dBZ, $P = -20\log_{10} r$. By applying this equation to the inner and outer rim of each range ring, it is possible to calculate the reflectivity increments which each ring should exhibit from ring's edge to ring peak. This effect is illustrated in Figures 1 and 2 and the increments are given in Table 8. It should be noted that the minimum detectable values differ with each radar, but the relative values represented by the increments should remain constant.

Table 8. Computed increments in reflectivity between minimum reflectivities for inner and outer boundaries of the range rings.

| Ring | Range (km) | Detectibility Increment (dBZ) |
|---|---|---|
| 1 | 1 - 32 | 30.1 |
| 2 | 32 - 64 | 6.0 |
| 3 | 64 - 96 | 3.5 |
| 4 | 96 - 128 | 2.5 |
| 5 | 128 - 160 | 1.9 |
| 6 | 160 - 192 | 1.5 |
| 7 | 192 - 224 | 1.4 |
| 8 | 224 - 256 | 1.2 |

These increments, however, will be augmented when attenuation is taken into account. This can be done by multiplying the correct attenuation factor (dependent on height, wavelength and season) by 32 km. to get a ring attenuation factor and then by multiplying the $\log_{10}$ of that quantity by 20 to get a realistic attenuation increment for each range ring.

## Results and Discussion

Summary of data and results.

This study is based on data taken at MIT's Weather Radar Laboratory during four different storms. The storms were chosen because of the variety they provided in structure and season. Included were two cyclonic storms, on September 24, 1975 and April 1, 1976, a squall line which passed Boston on August 13, 1976 and a broad area of pre-cold frontal rain which centered on a very long and narrow line of heavy rain on December 7, 1976. In addition, both radars available in the laboratory are represented in these storms; the majority of data on the August and September storms was recorded on the WR73, while the other storms were observed using the WR66. In each case, a true sampling was sought by analyzing anywhere from four to seven individual maps at time intervals of one half hour. This was, of necessity, a flexible requirement because of the irregularity with which maps with a sufficient number of elevation angles were recorded.

Information concerning range effects can best be obtained through careful study of the observed distributions and behavior of individual range rings. The best format for this type of study is a graph of the fraction of data points in each ring which lie within a specified reflectivity interval versus the reflectivity factor. Such graphs can be made by plotting data which has been corrected for attenuation from the summary tables of each storm so that comparisons can be made

from storm to storm and from height to height. These graphs for all heights and range rings for the storm totals can be found in Figures 6 through 17.

A careful study of these results reveals the strong resemblance which exists between these graphs and the models in Figures 1 and 2. The models illustrate the expected effects of the variation of minimum detectable signal with range. The August and September storms (Figures 6 through 11) most clearly resemble the sloping model which is illustrated in Figure 1. These graphs show the relation between the minimum detectable value for the outer boundary and the inner boundary of a given range ring which is discussed in Chapter 1. The curves rise sharply from the minimum detectable reflectivity for the inner boundary of the range ring until they meet the real distribution at the minimum detectable reflectivity of the outer boundary. In addition, the resemblance to Figure 1 indicates a typical storm with relatively large areas of light rain.

The resemblance which exists between Figure 2, or the peaked model, and the December and April storms (Figures 12 through 17) also reflects the relation described above, which exists between the minimum detectable value for the outer boundary and the inner boundary of the range ring. However, the peaked nature of these graphs indicates that the storms have a preferred rainfall rate at a somewhat higher reflectivity which varies from height to height.

However, certain discrepancies also exist between the

models and the actual graphs. These include the unusual behavior which Rings 1 and 2 exhibit in almost every storm and the deviant structure of the rings at high reflectivities. Instead of the rings coinciding at high reflectivities as illustrated in the model, the rings drop off to varied reflectivity values. This variance results in the rings ending at either progressively higher (See Figure 14) or lower (See Figure 12) reflectivity values as the range increases. A discussion of possible explanations of these effects and others follows.

Effects of minimum detectable signal.

As previously mentioned, a strong resemblance exists between Figure 1 or the sloping model and the August and September storms. Further evidence of the similarity can be found through examination of the reflectivity value increment from a given ring's lowest reflectivity value to its "peak" value, or the value which corresponds to largest coverage. Table 9 presents a comparison of these increments with those calculated in Chapter 2 which represent the differences in the minimum detectable values of reflectivity for the inner and outer boundary of each range ring. With attenuation taken into account, the increments show a variance of no more than one or two dBZ.

These results substantiate the argument concerning the sloping model which was presented in Chapter 1. That is, at the intensity representing the minimum detectable value for the outer boundary of a given range ring, the observed frequency

begins to drop away from the actual one, reaching a low at the minimum detectable value for the inner boundary.

Table 9. Observed and computed increments in reflectivity between minimum reflectivities for inner and outer boundaries of the range rings.

August 13, 1976

| Ring | Low Value(dBZ) | Peak(dBZ) | Increment(dBZ) | Computed Increment ± Attenuation(dBZ) |
|---|---|---|---|---|
| 2 | 15 | 21 | 6 | 6.4 |
| 3 | 21 | 24 | 3 | 3.9 |
| 4 | 25 | 27 | 2 | 2.8 |
| 5 | 27 | 29 | 2 | 2.3 |
| 6 | 29 | 31 | 2 | 1.8 |
| 7 | 31 | 33 | 2 | 1.8 |

September 24, 1975

| Ring | Low Value(dBZ) | Peak(dBZ) | Increment(dBZ) | Computed Increment ± Attenuation(dBZ) |
|---|---|---|---|---|
| 2 | 13 | 19 | 6 | 6.4 |
| 3 | 18 | 22 | 4 | 3.9 |
| 4 | 23 | 25 | 2 | 2.8 |
| 5 | 25 | 27 | 2 | 2.3 |
| 6 | 27 | 29 | 2 | 1.8 |
| 7 | 29 | 29 | 0 | 1.8 |

The remaining storms more closely resemble the peaking model of Figure 2. Because of the nature of the model, individual ring "peaks" do not exist. Therefore, comparisons are made between the minimum detectable increments calculated in Chapter 2 and the increments which exist between the lowest reflectivity values of adjacent rings. These results are presented in Table 10.

Here again, agreement is close, within 2 dBZ. These results indicate that the peaking model illustrated in Figure 2 is a viable model for predicting the expected effect of the increase of the minimum detectable value of reflectivity with an increase in range. This model is restricted, however, to storms which exhibit a preferred rainfall rate at a relatively

high reflectivity.

Table 10. Same as Table 9.

April 1, 1976

| Ring | Low Value(dBZ) | Increment(dBZ) | Computed Increment ± Attenuation(dBZ) |
|---|---|---|---|
| 2 | less than 11 | >4 | 6.3 |
| 3 | 15 | 4 | 3.8 |
| 4 | 19 | 3 | 2.8 |
| 5 | 21 | 2 | 2.2 |
| 6 | 23 | 2 | 1.8 |
| 7 | 25 | | |

December 7, 1976

| Ring | Low Value(dBZ) | Increment(dBZ) | Computed Increment ± Attenuation(dBZ) |
|---|---|---|---|
| 2 | 13 | 4 | 6.3 |
| 3 | 17 | 4 | 3.8 |
| 4 | 21 | 2 | 2.8 |
| 5 | 23 | 3 | 2.3 |
| 6 | 26 | 2 | 1.8 |
| 7 | 28 | | |

Effects of ground echoes.

Among the discrepancies noted earlier between the graphed results and models was the unusual behavior apparent in Rings 1 and 2 in different storms and at different heights. The variations ranged from the towering peaks evident in Figure 17 to the plateaus of Figure 6 to the absence of Rings 1 and 2 in Figure 14. There are a number of possible explanations for these anomalies. The most likely explanation is the effect of ground echoes. Rings 1 and 2 lie so close to the radiation source that, for low elevation angles, the beam intercepts tall buildings and land elevations and reflects them back as actual data points. That data then gets recorded and processed as if they were precipitation echoes. The result is distorted data from Rings 1 and 2 which cause discrepancies in the distribution curves.

For higher elevation angles, ground targets are eliminated but the strange shape of the distribution curves can instead be traced to non-representative sampling. The total area of Rings 1 and 2 is relatively small so that if any precipitation feature is present in just one ring, it has a high fractional coverage, and thus causes a narrow distribution curve (See Figure 17). Also at higher levels, light precipitation, which tends to be fairly continuous, may cover most of the area and be detectable in the inner rings, resulting in a very high percentage of coverage. However, this light rain would not be detectable at farther distances, thus the distribution in the outer rings follows the proposed models more closely.

Finally, a major discrepancy which concerns Rings 1 and 2 is the fact that often they do not appear at all. This is a direct result of the manner in which the data were collected for each particular storm. Often data collection begins on the outside rim of Ring 1 or 2 to avoid the ground clutter and other effects mentioned above. Alternatively, sometimes data is just collected at low elevation angles, especially in winter storms where precipitation is most likely to occur at low levels. Thus the scan never reaches high heights in Rings 1 and 2 and therefore no data is recorded in them (See Figure 14).

Effects of beam width

The other discrepancy from the proposed models which was mentioned earlier was that the rings do not coincide at higher reflectivities as hypothesized in the model. Instead, the ends of the rings seem to progress somewhat steadily from lower to

higher reflectivities or vice versa as the ring number diminishes.

One reason for continuously larger range rings to end on progressively larger reflectivities is the effect of beam width. In the case where Z decreases with height across a given layer as well as above and below it, the measured distribution is affected at far ranges where the beam is broader. The results are: (1) for sample points where the center of the beam coincides fairly closely with the center of the layer, the distribution remains essentially unchanged; (2) for sample points where the center of the beam comes close to the bottom of the layer, there appears a higher Z because some of the beam extends downward into the higher reflectivity layer below; and (3) for sample points where the center of the beam comes close to the top of the layer, there is a similar downward shift in the distribution. The net result of these three effects in an observed distribution would be for the high reflectivity tail to broaden out, causing the middle and lower portions to be diminished slightly. The effect on the lower and middle portions is due to the fact that each ring has a finite number of points, thus the broadening at the high end must be compensated for in other areas of the ring.

Accompanying this outward motion by the tails is a similar motion by the peaks. This effect can be traced to the fact that the minimum detectable effect cuts in before the results of the lowering peak and broadening ends can be seen, thus creating the appearance of the peaks moving outward (See Figure 14).

In the case where the opposite movement takes place, that

is where continuously larger range rings end on progressively smaller reflectivities, a melting layer effect can be hypothesized. For example, if the melting layer is near the top of the 2 km. layer, at far ranges a broader beam will extend above the bright band into the snow. The result is a lower average reflectivity value for points where the beam center is near the top of the layer. However, due to the structure of the melting layer, there is no compensating increase when the beam center nears the bottom of the layer. The net effect is, therefore, a lowering of reflectivity values at the ends of progressively larger rings. This tendency is most noticeable in the 2 km. layer (See Figure 12).

Another beam width effect which is noticeable is the sudden drop in coverage which Ring 7 and occasionally Ring 6 exhibit in relation to the other rings (See Figure 13). The reason for this is that, at far ranges, the broader beam increases the volume of atmosphere sampled and causes the individual values to smear. Thus it is possible that even if there are small intense showers taking place in Ring 7, these values will be averaged over a larger area, causing the peak values to be reduced.

A final anomaly which is noticeable in Rings 6 and 7 is that often the peaks in these two rings occur at the same reflectivity interval (See Figure 7). This effect may be due to a single intense precipitation area which spans the outer edge of Ring 6 and the inner edge of Ring 7 and thus provides an identical peak reflectivity for both rings.

Variations of reflectivity with height.

The way in which the data from this study is structured lends itself not only to range comparisons, but height comparisons as well. A study of graphs on which the same range rings at different heights are plotted for the same storm indicates that, for the most part, the storms behave as expected (See Figures 18 to 33). That is, there is a broad coverage of a wide range of reflectivities at lower levels; a sharpening and narrowing of the spectrum at middle levels, indicating less variation in storm structure at that height; and then usually a sharp drop in intensity for the higher levels, most likely indicative of a cross over the melting layer and into less highly reflective snow. Sometimes, however, as in the August storm (See Figure 23), the higher levels show signs of good coverage in the middle reflectivity values. This is most likely to signal the anvil structure connected with thunderstorms.

## Conclusion

The results of this study indicate that range dependent effects such as attenuation, resolution and minimum detectable signal are of sufficient magnitude to affect observed intensity distributions. For this reason, they should be considered whenever radar data are used. Attenuation by atmospheric gases, in particular, is of sufficient significance and constancy to be included as a matter of course in the data processing which takes place prior to any analysis.

Although they are not as easy to quantify as attenuation, it is encouraging to find the degree to which some of the other effects are at least predictable. The minimum detectable signal effect, especially, follows the proposed models to a large extent, with each range ring showing less and less light precipitation while the peaks for each ring move to higher reflectivity factors and lower area coverage. The existence of ground echoes and other short range effects was evident, as predicted, in the distorted shapes of Rings 1 and 2. Finally, the beam spread effect proved to be fairly observable and consistent, causing a broadening of the high reflectivity tail at high heights and a retreat at low heights.

The clarification of these properties should make future detection easier. Unfortunately, as mentioned before, they are difficult to quantify. It is impossible to devise a general rule or formula for replacing what is lost to these

effects because the actual distributions vary from storm to storm, and there are also variations of reflectivity with height. Instead, when statistical experiments are undertaken, an effort must be made to prevent these observed effects from invalidating the results.

Areas which require further consideration include the effect on signal statistics of the loss of energy below the horizon at low elevation angles and investigation into the various ways in which the melting layer may affect radar data. The constant-height analysis described in this study is ideal for such investigation because the height interval containing the phenomenon under consideration can be narrowed or widened as desired to facilitate either detailed or broad analysis. Constant-height analysis is also important in more general terms for the information it reveals concerning storm structure at various levels.

This type of information was not easily discerned from the scope displays previously used for all radar research, but now, with the increased availability of digitally recorded data, a wide variety of statistical information can be gathered. This thesis shows, however, that care must be taken to provide for range and other effects when in-depth analysis of this information is performed.

Figures 6 through 17 are graphs of the summary tables for the nominal heights of 2, 4, and 6 km. for four different New England storms. The key to the graphs is as follows:

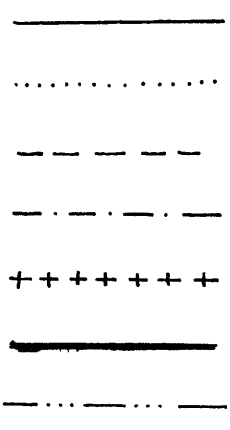

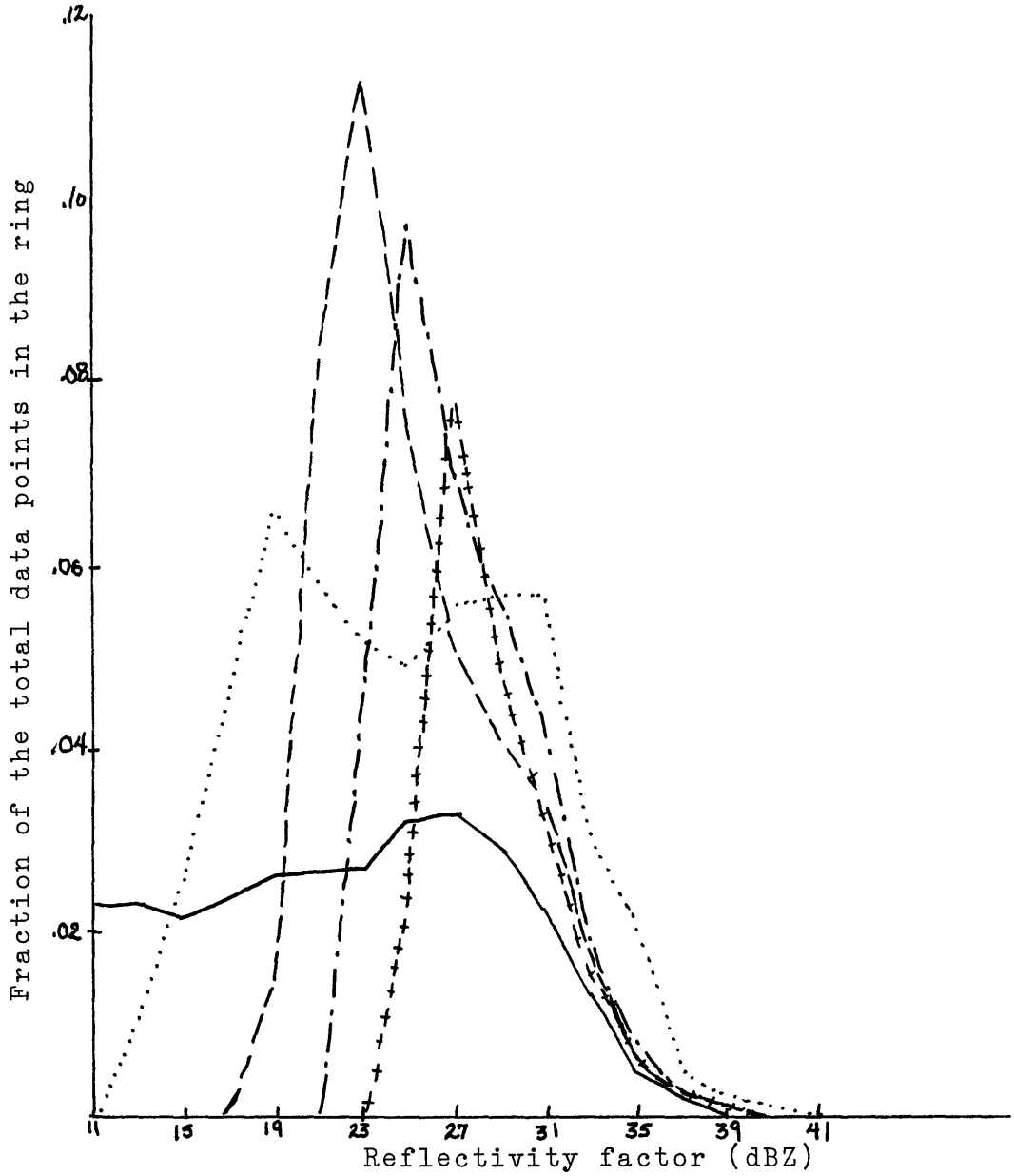


Figure 6. September 24, 1975, height = 2 km.

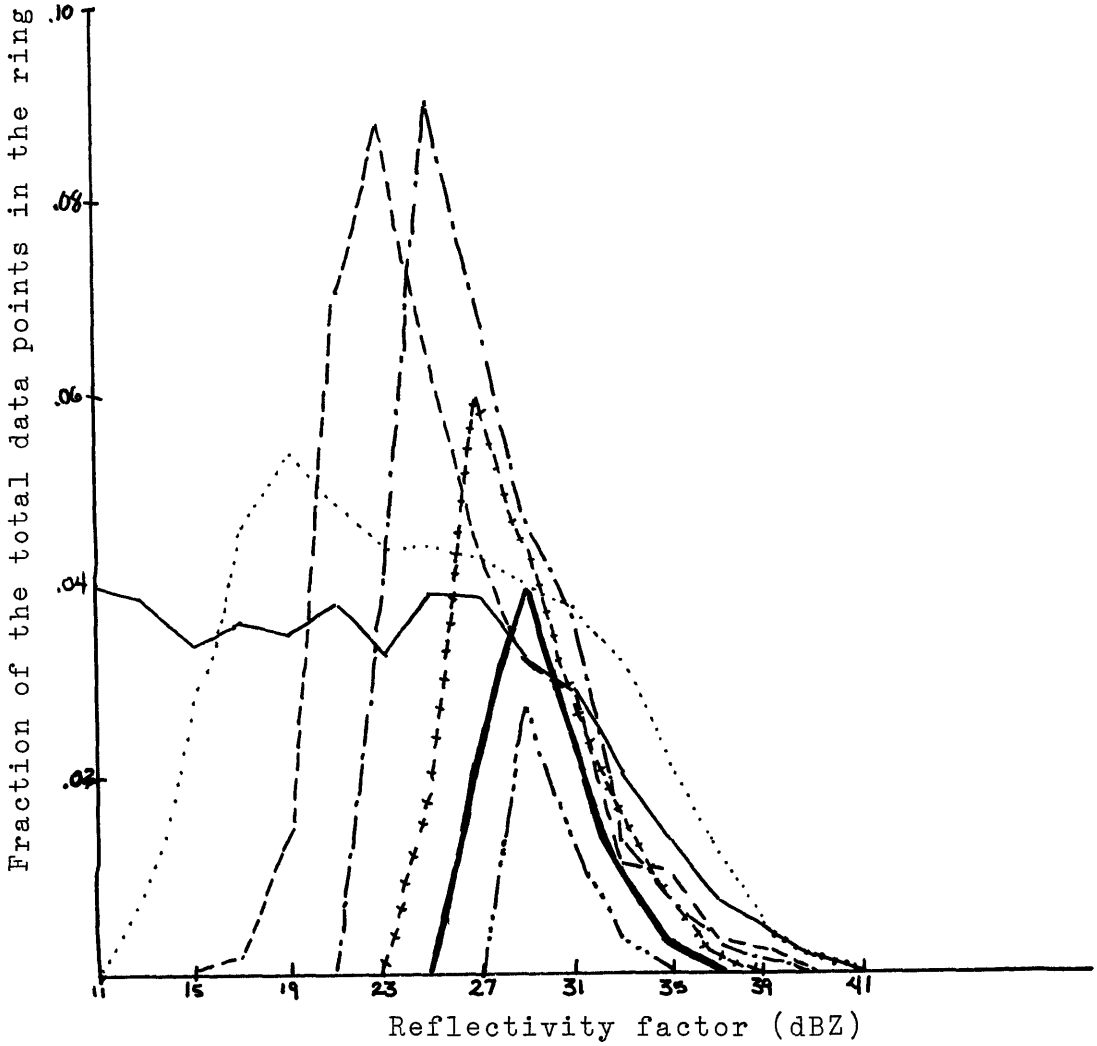


Figure 7. September 24, 1975, height = 4 km.

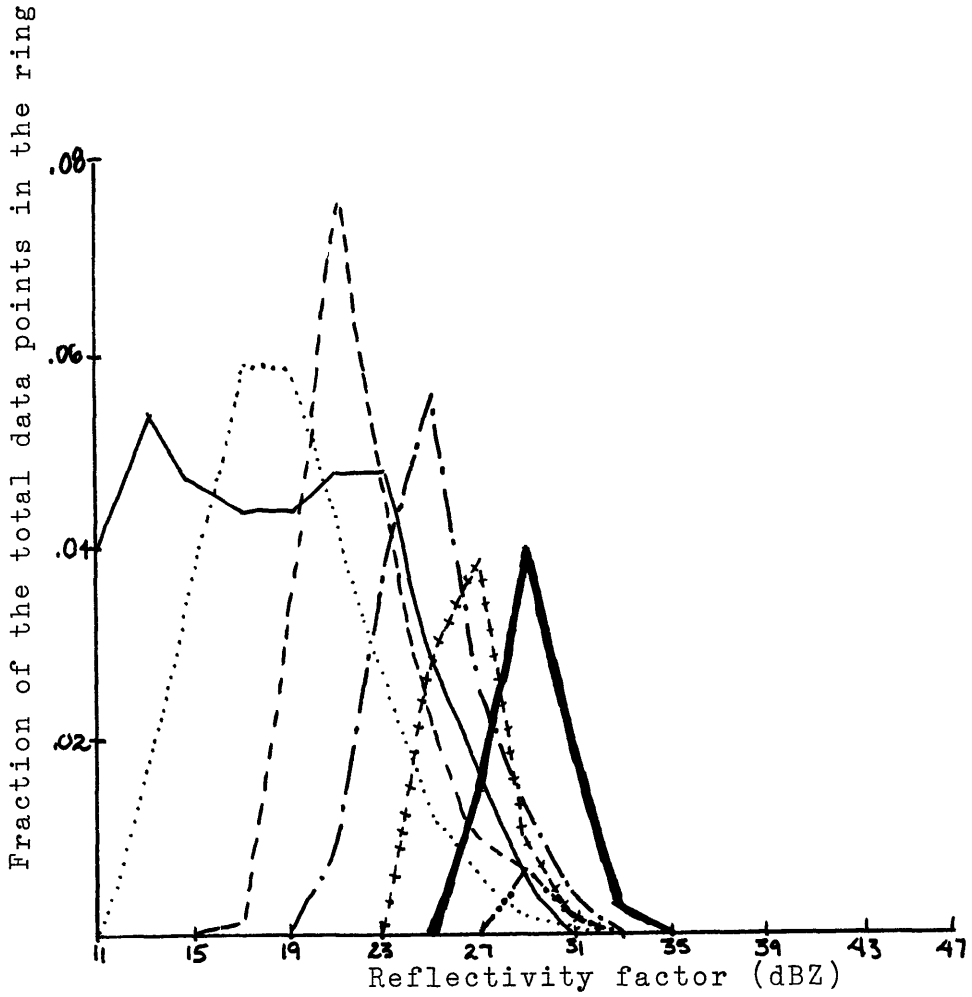


Figure 8. September 24, 1975, height = 6 km.

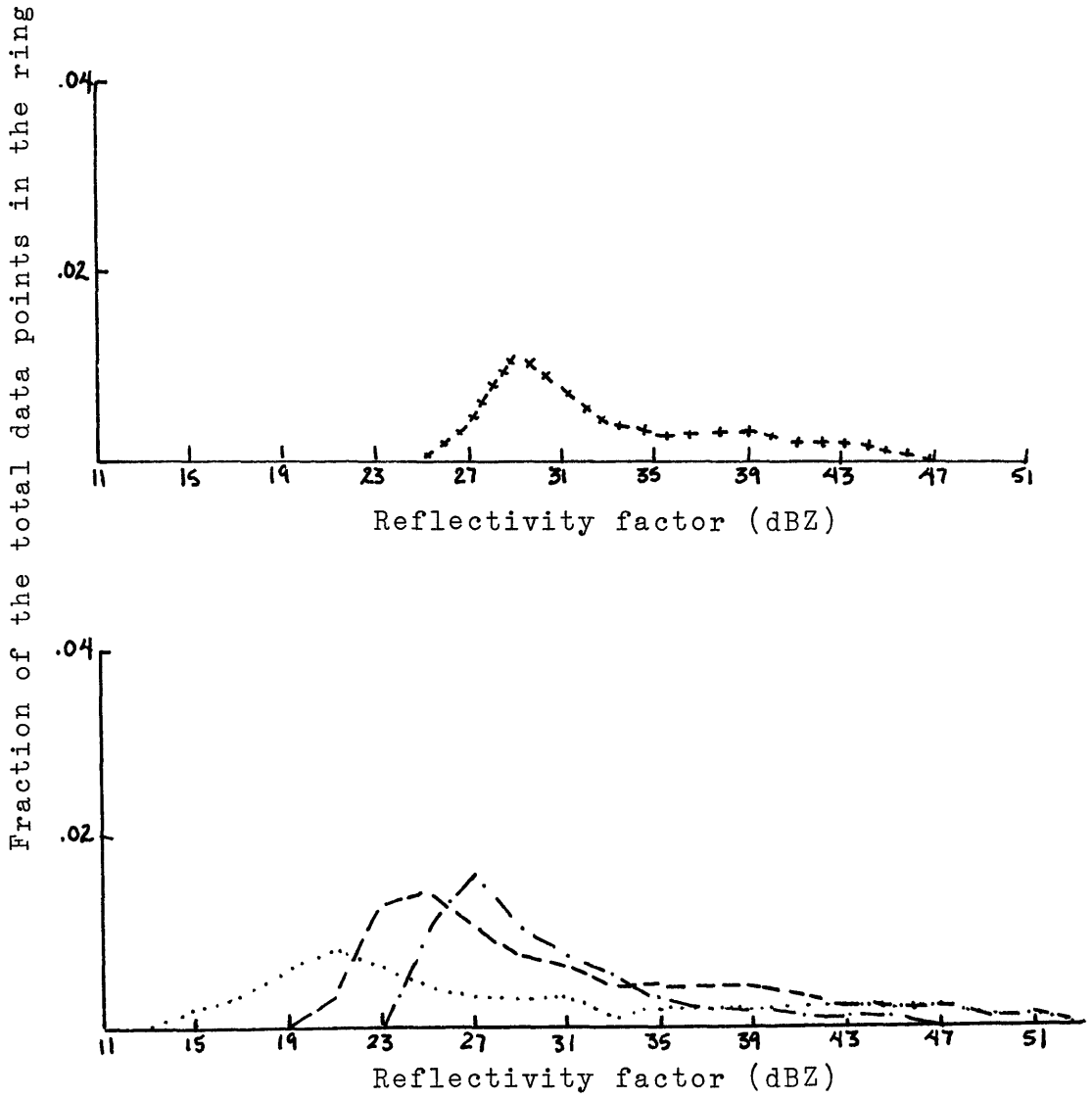


Figure 9. August 13, 1976, height = 2 km.

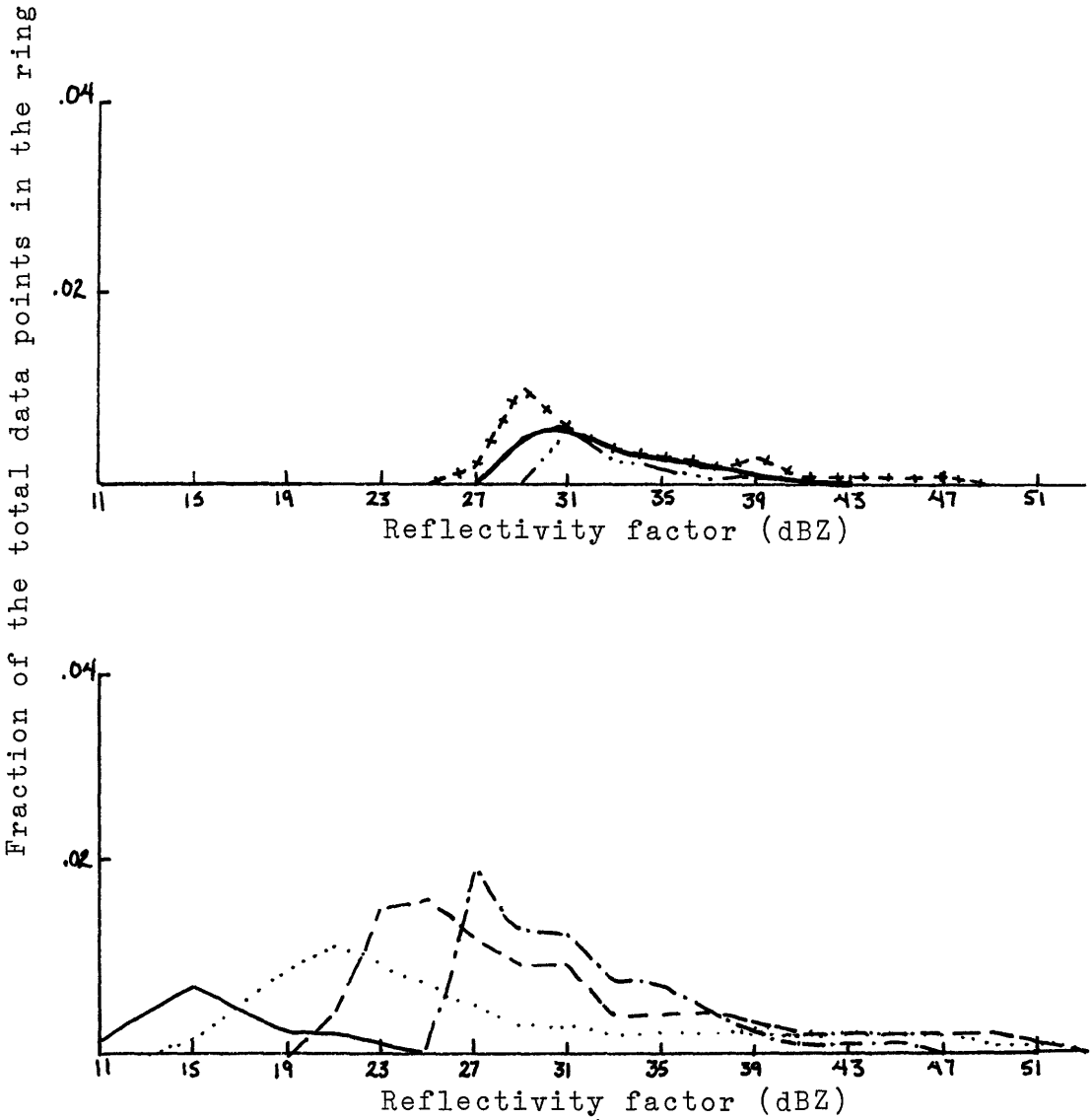


Figure 10. August 13, 1976, height = 4 km.

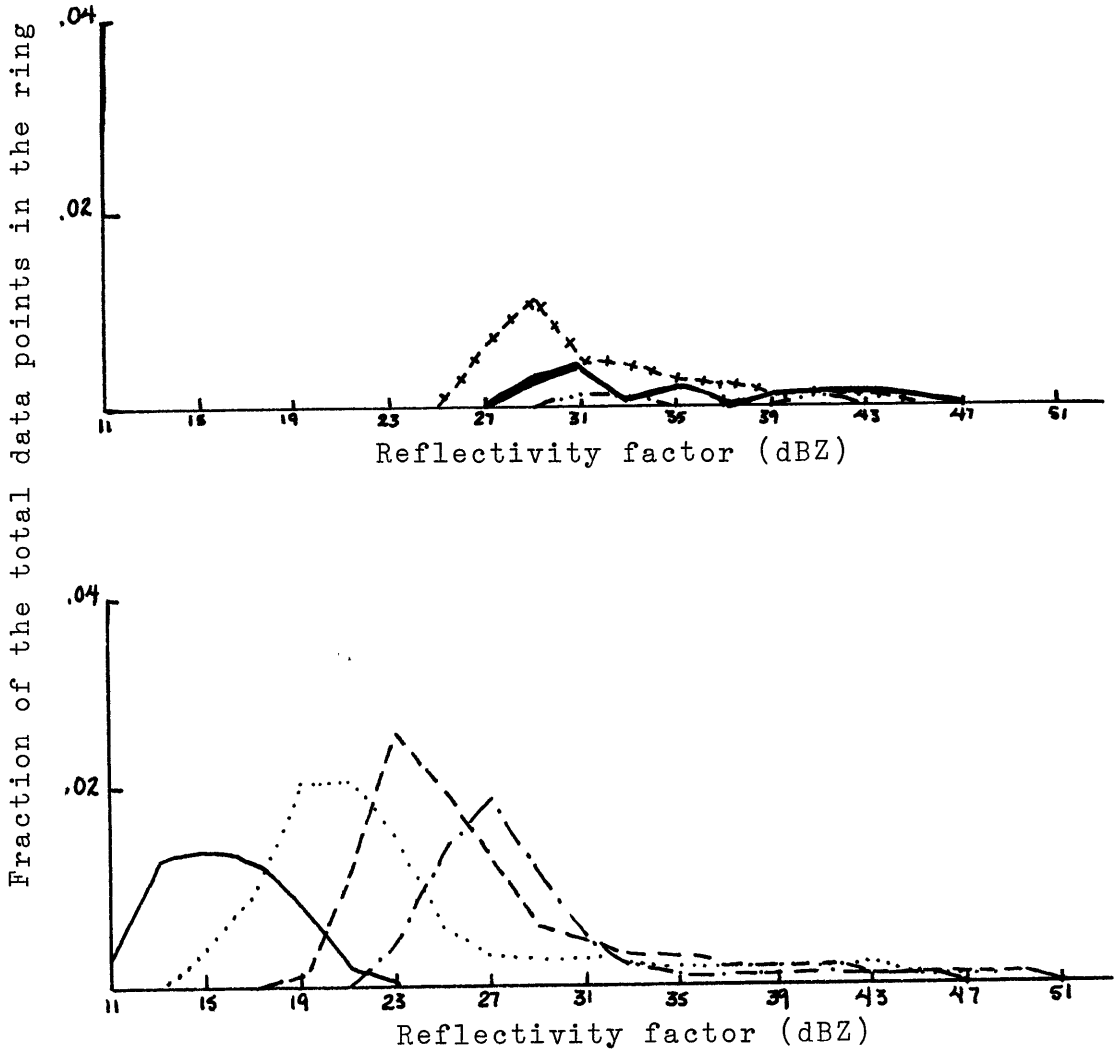


Figure 11. August 13, 1976, height = 6 km.

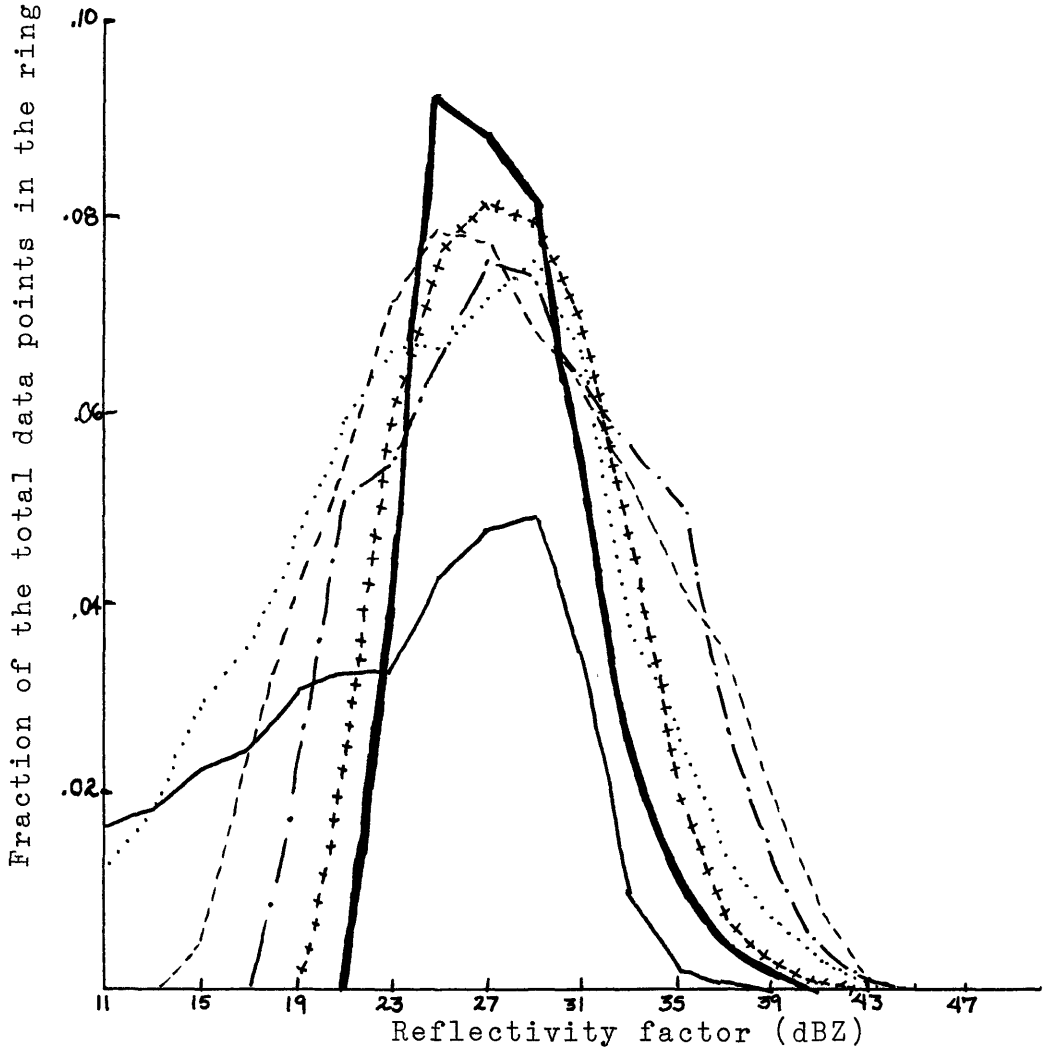


Figure 12. April 1, 1976, height = 2 km.

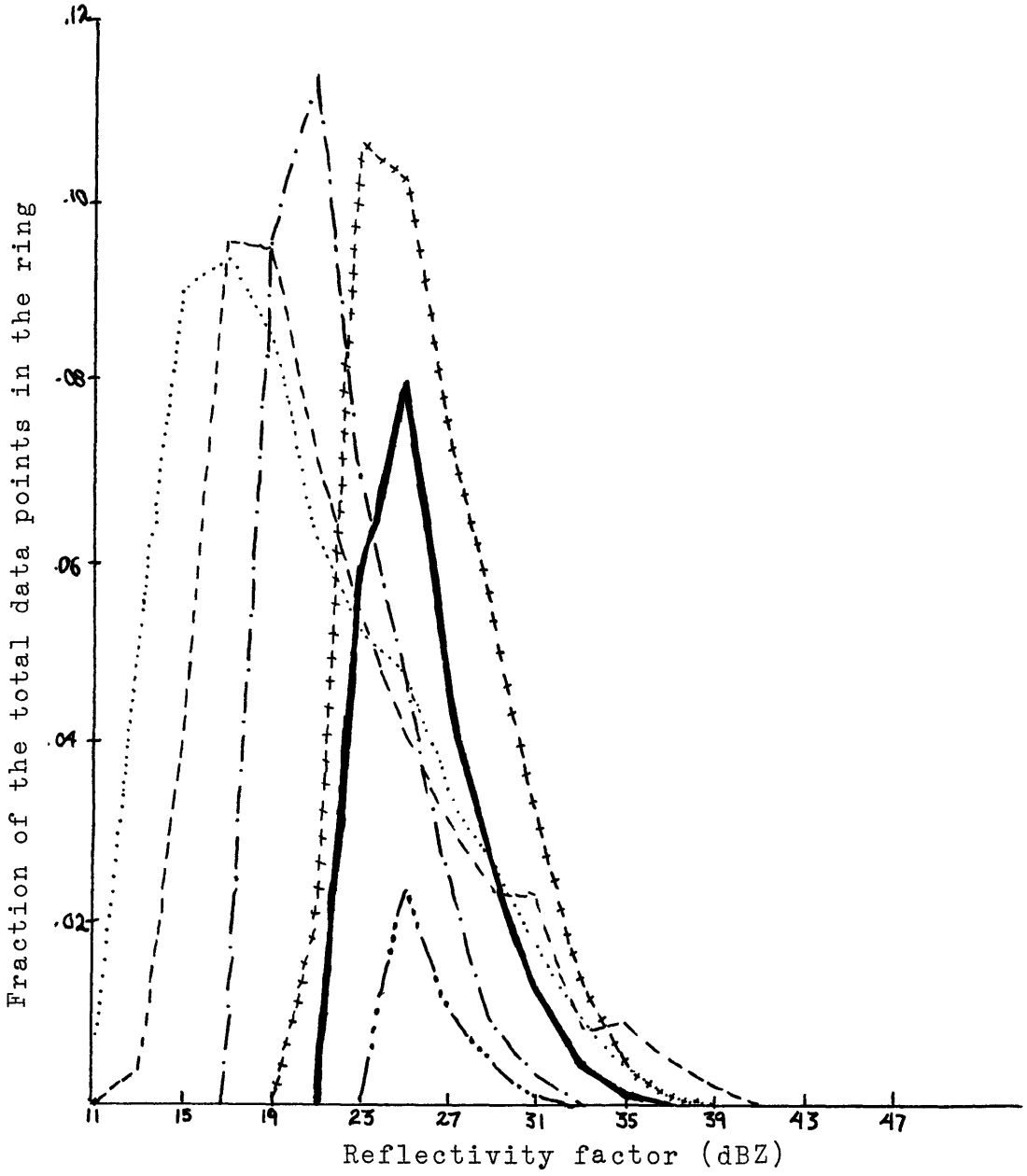


Figure 13. April 1, 1976, height = 4 km.

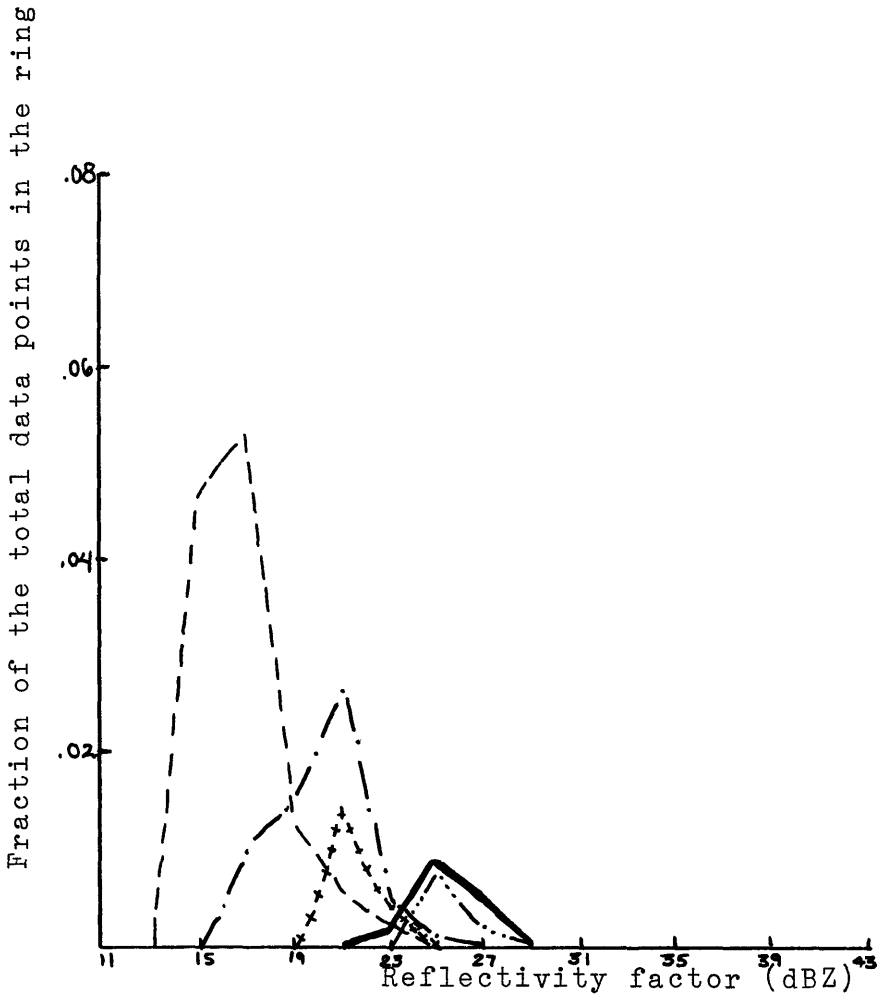


Figure 14. April 1, 1976, height = 6 km.

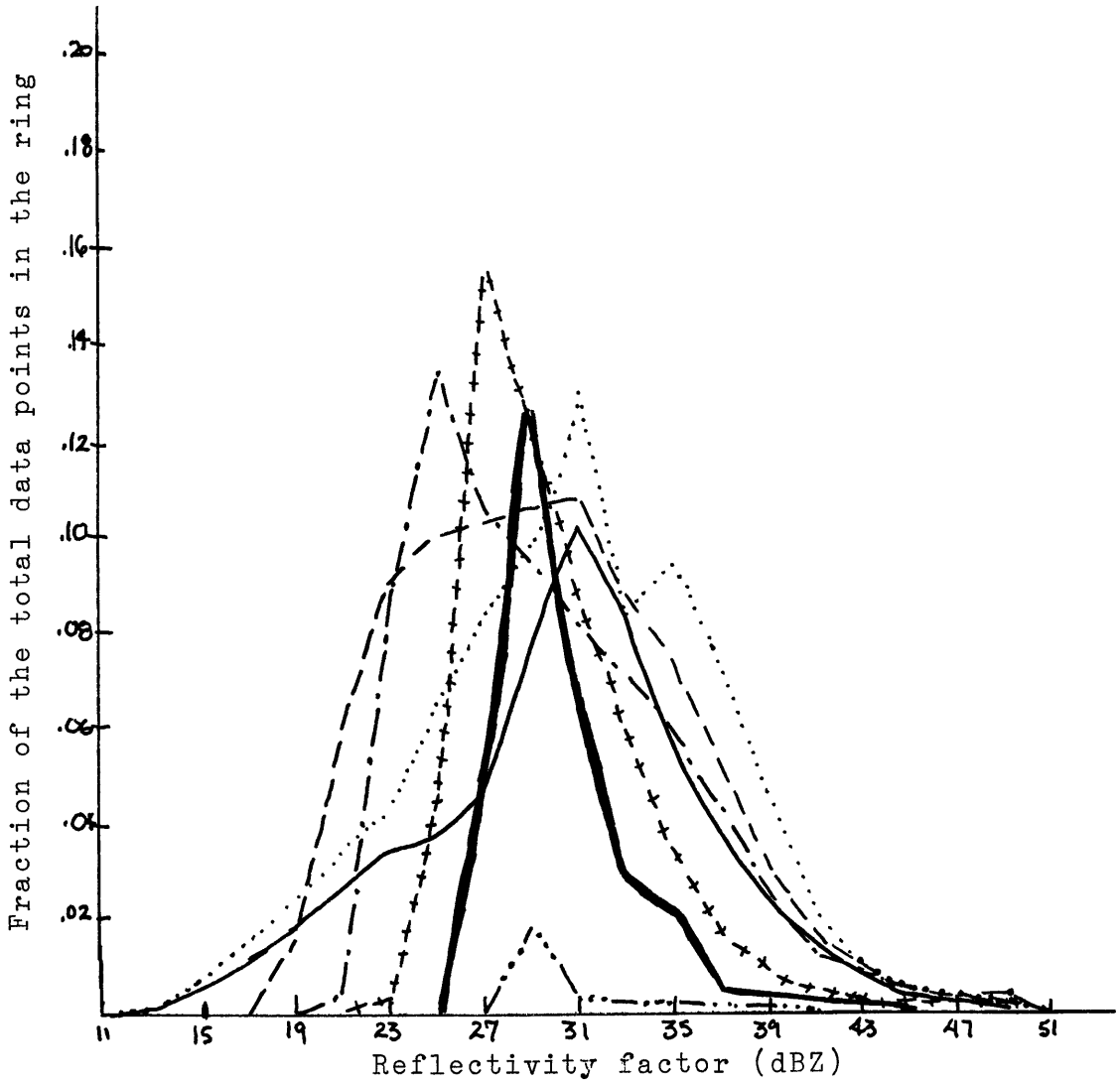


Figure 15. December 7, 1976, height = 2 km.

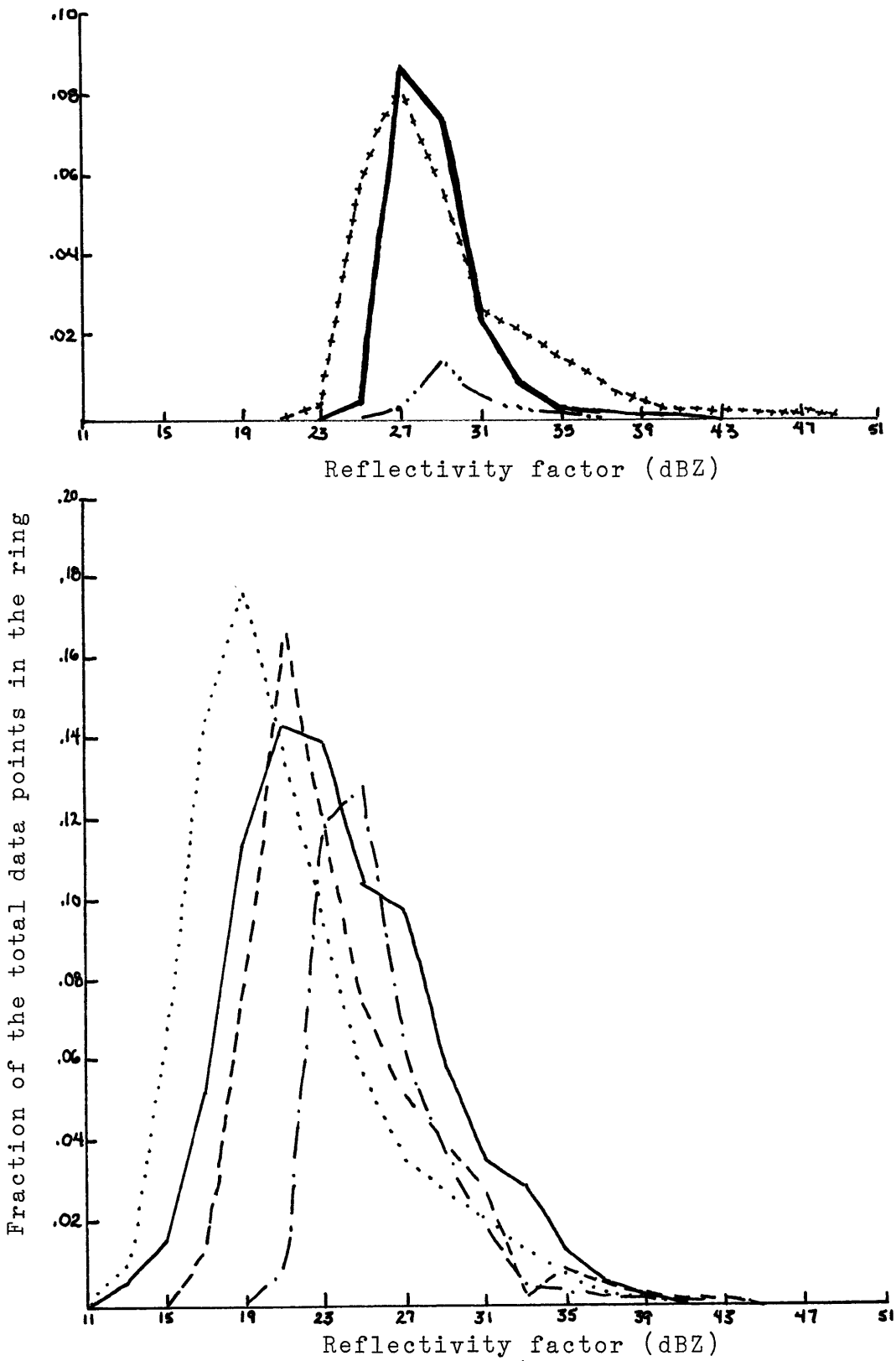


Figure 16. December 7, 1976, height = 4 km.

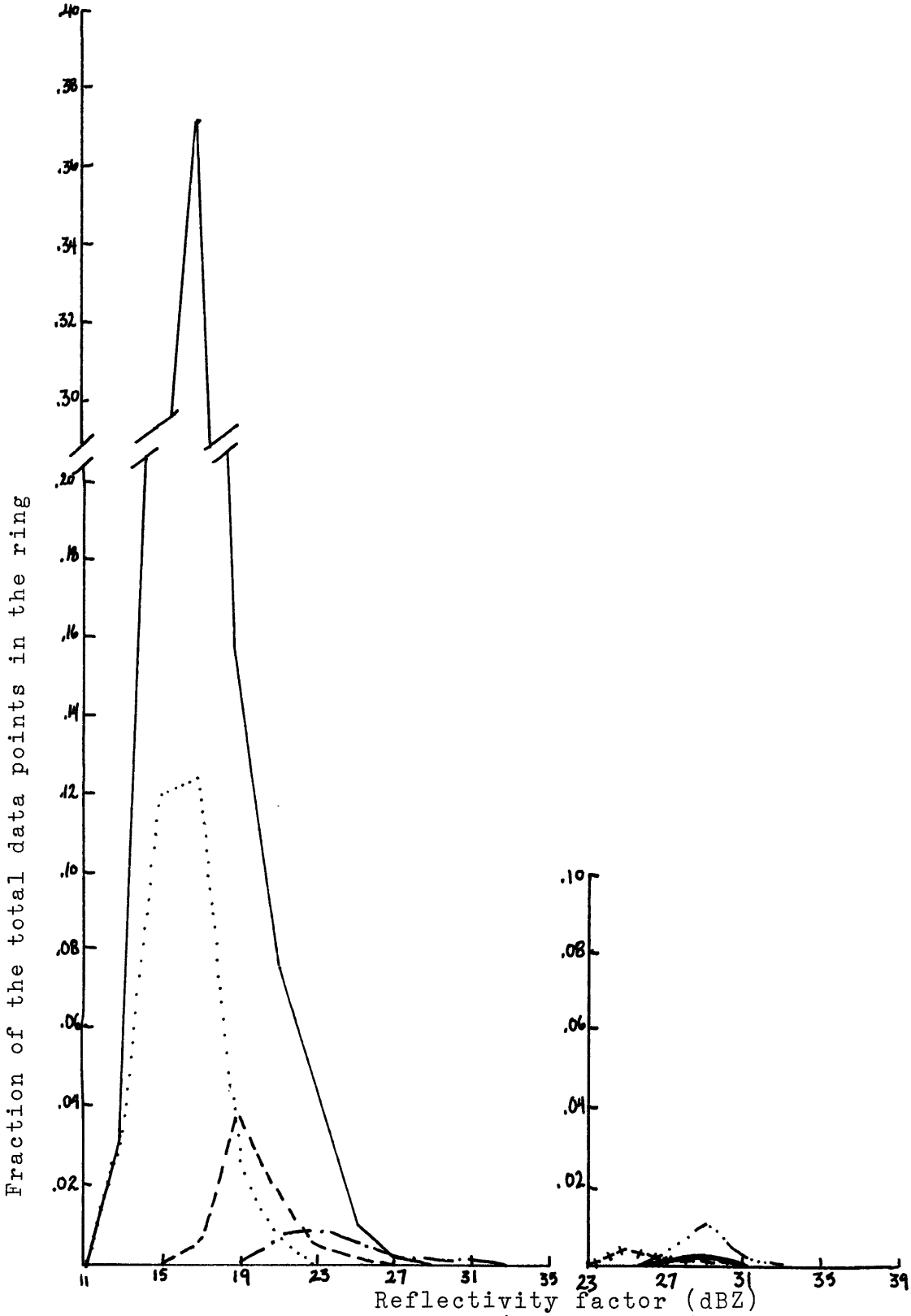


Figure 17. December 7, 1976, height = 6 km.

Figures 18 through 33 are graphs of specific range rings at heights of 2, 4 and 6 km. They were made using the data from the storm summary tables. The key to the graphs is as follows:

— — — — 2 km.

———— 4 km.

— · — · — 6 km.

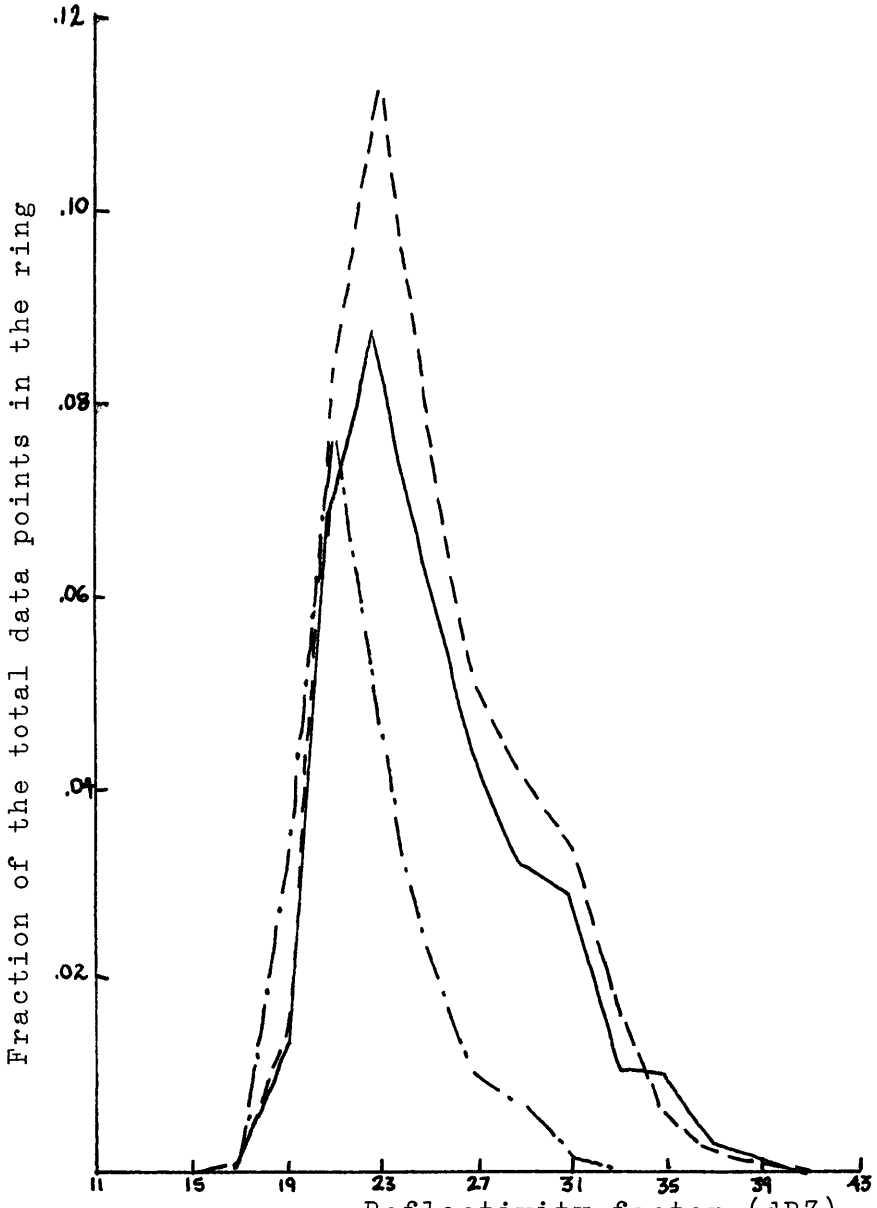


Figure 18. September 24, 1975, Ring 3.

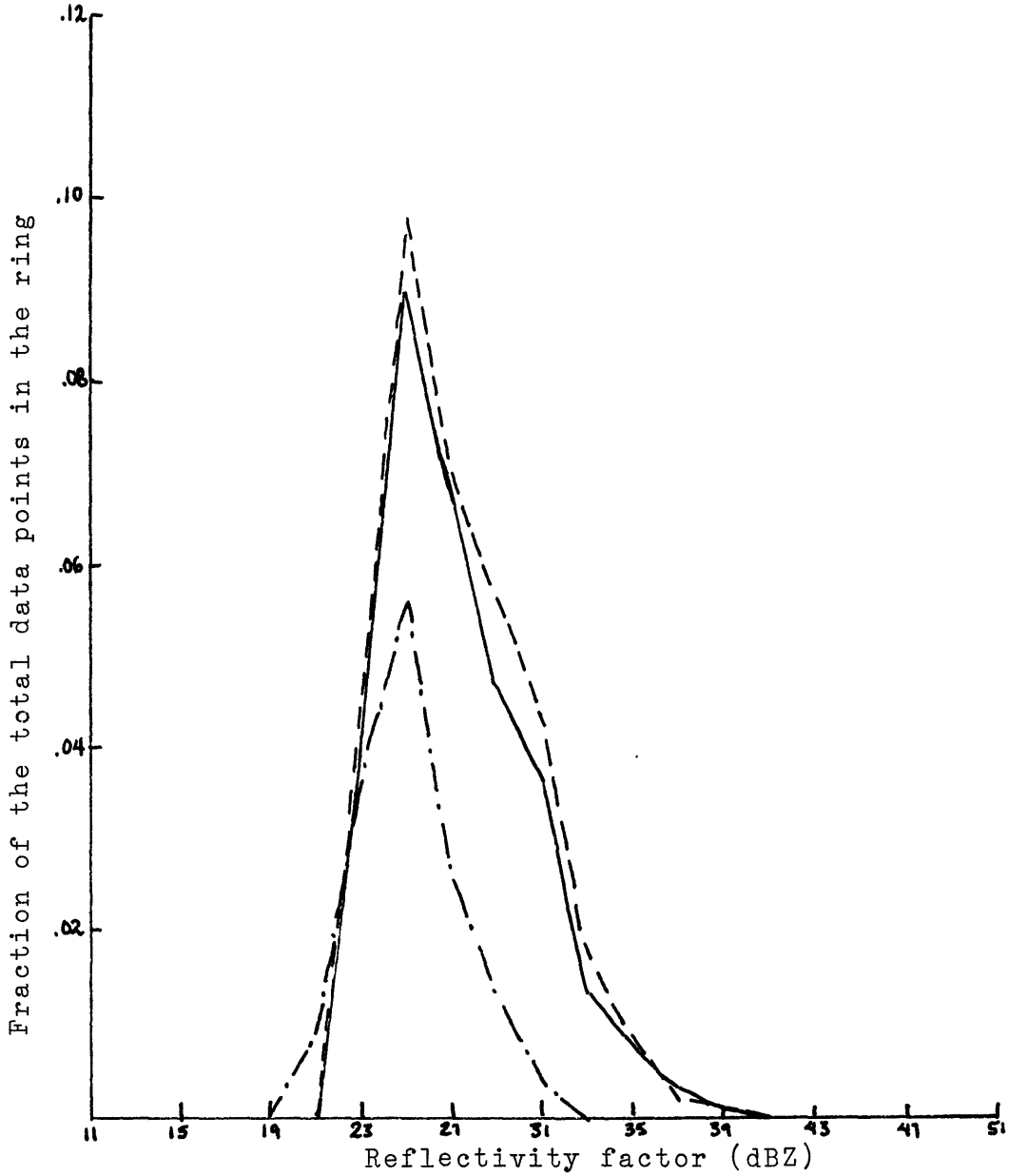


Figure 19. September 24, 1975, Ring 4.

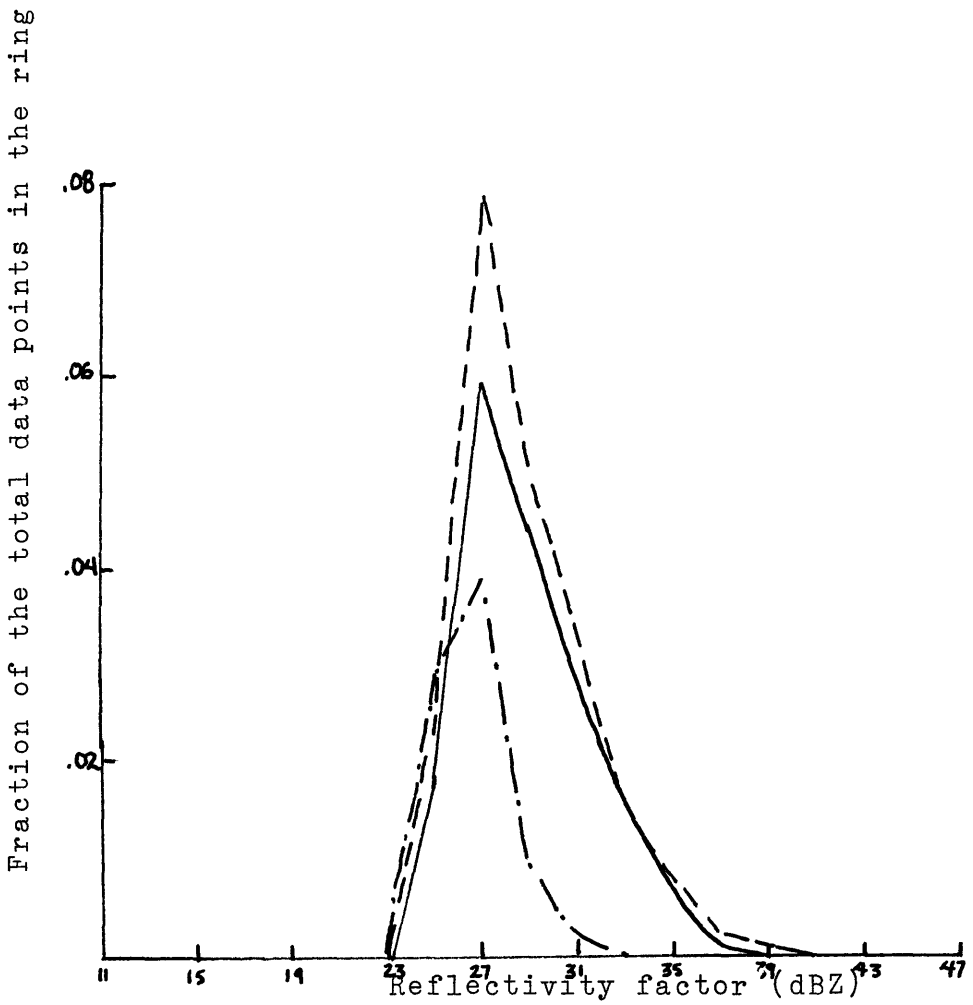


Figure 20. September 24, 1975, Ring 5.

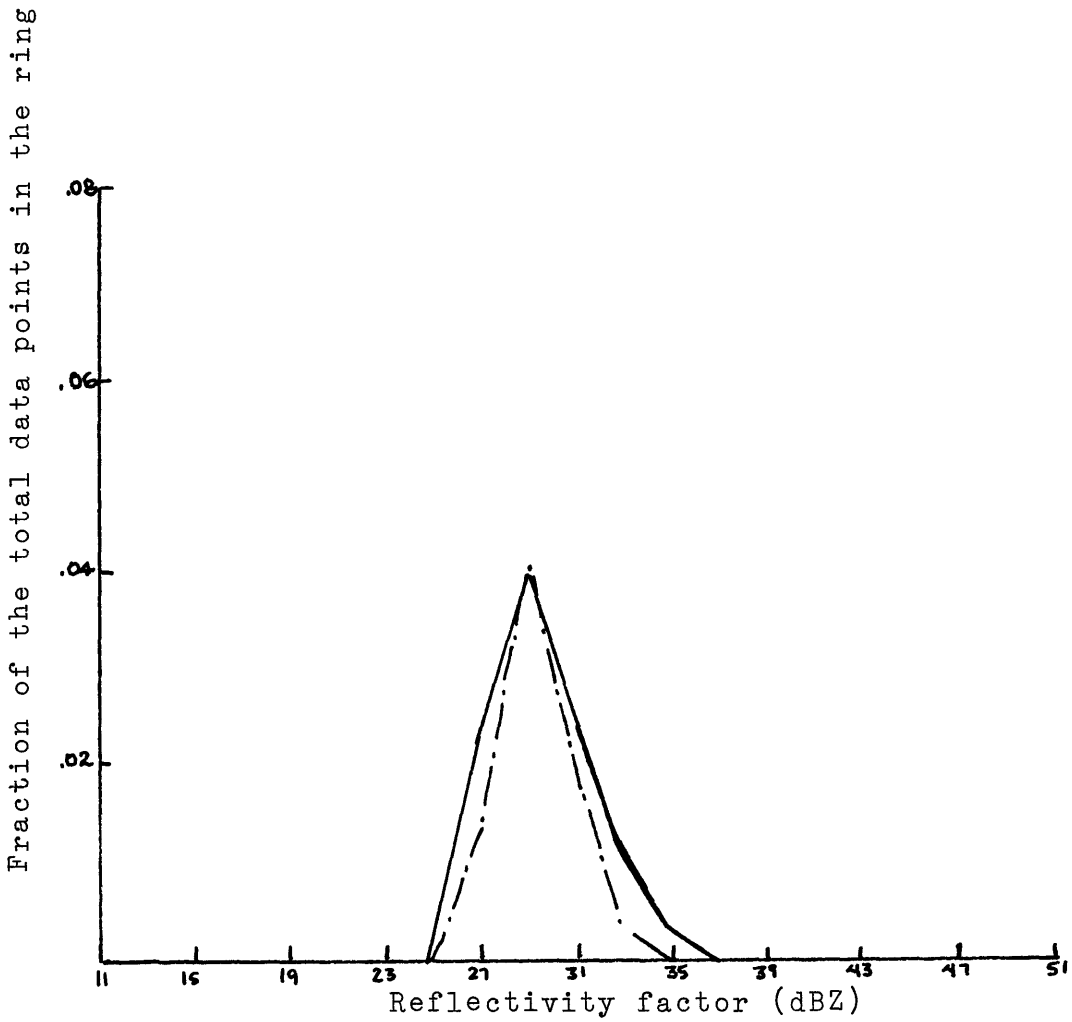


Figure 21. September 24, 1975, Ring 6.

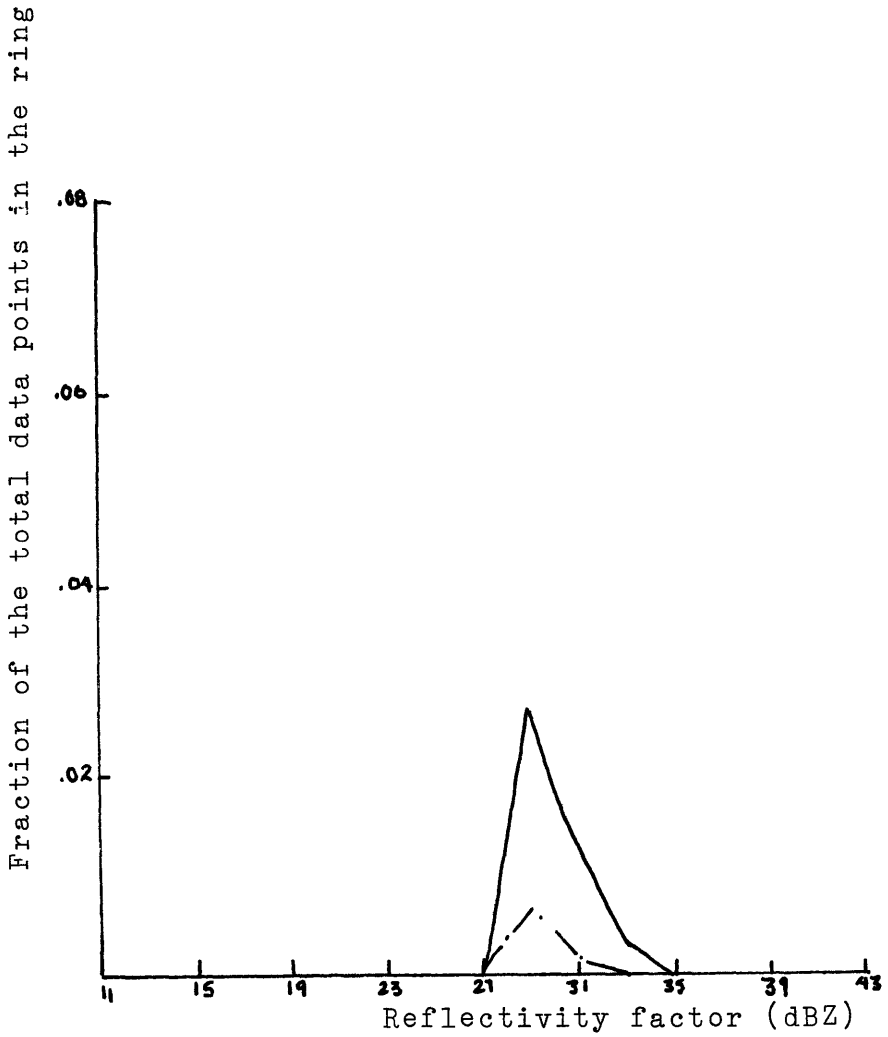


Figure 22. September 24, 1975, Ring 7.

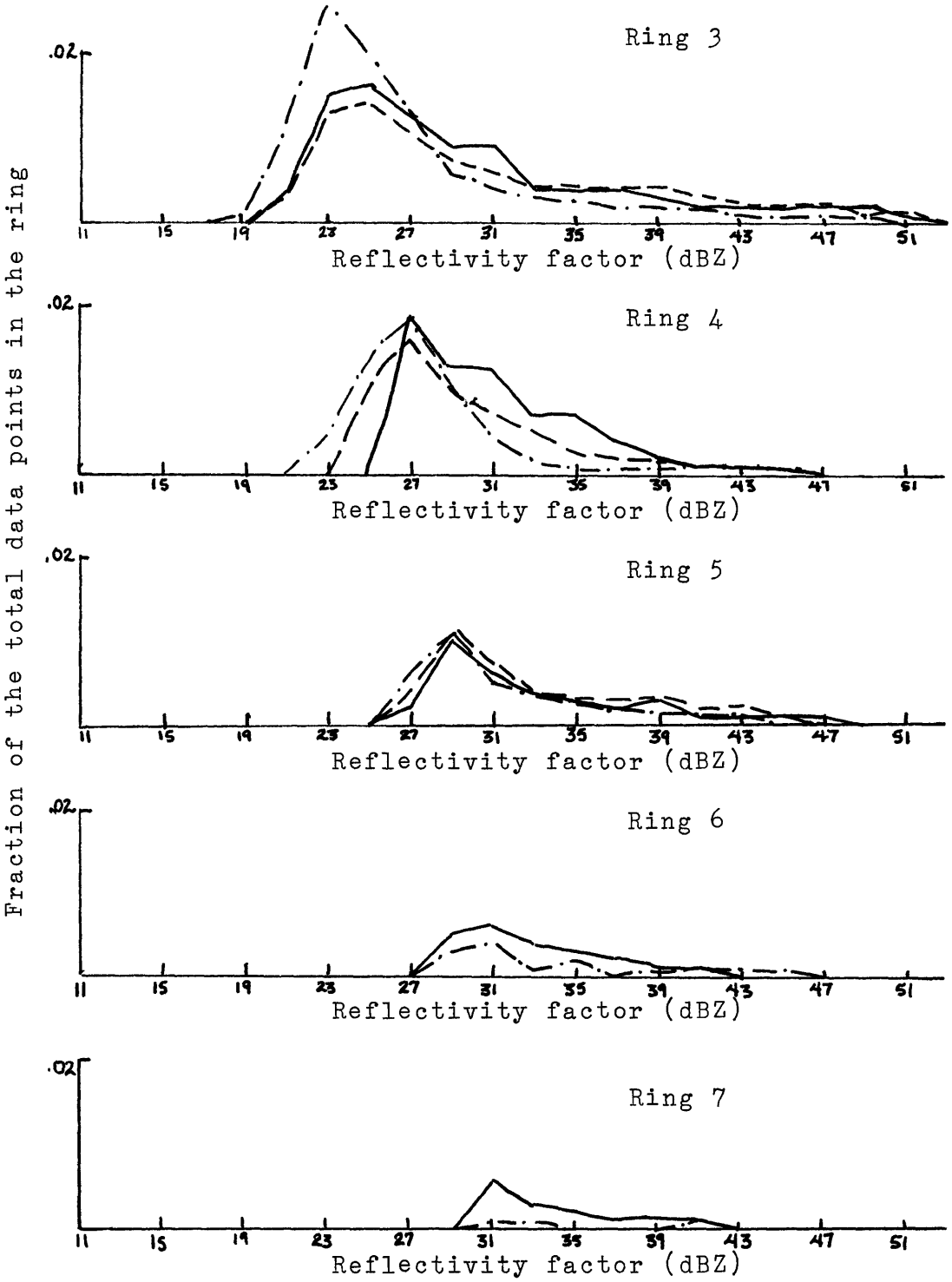


Figure 23. August 13, 1976.

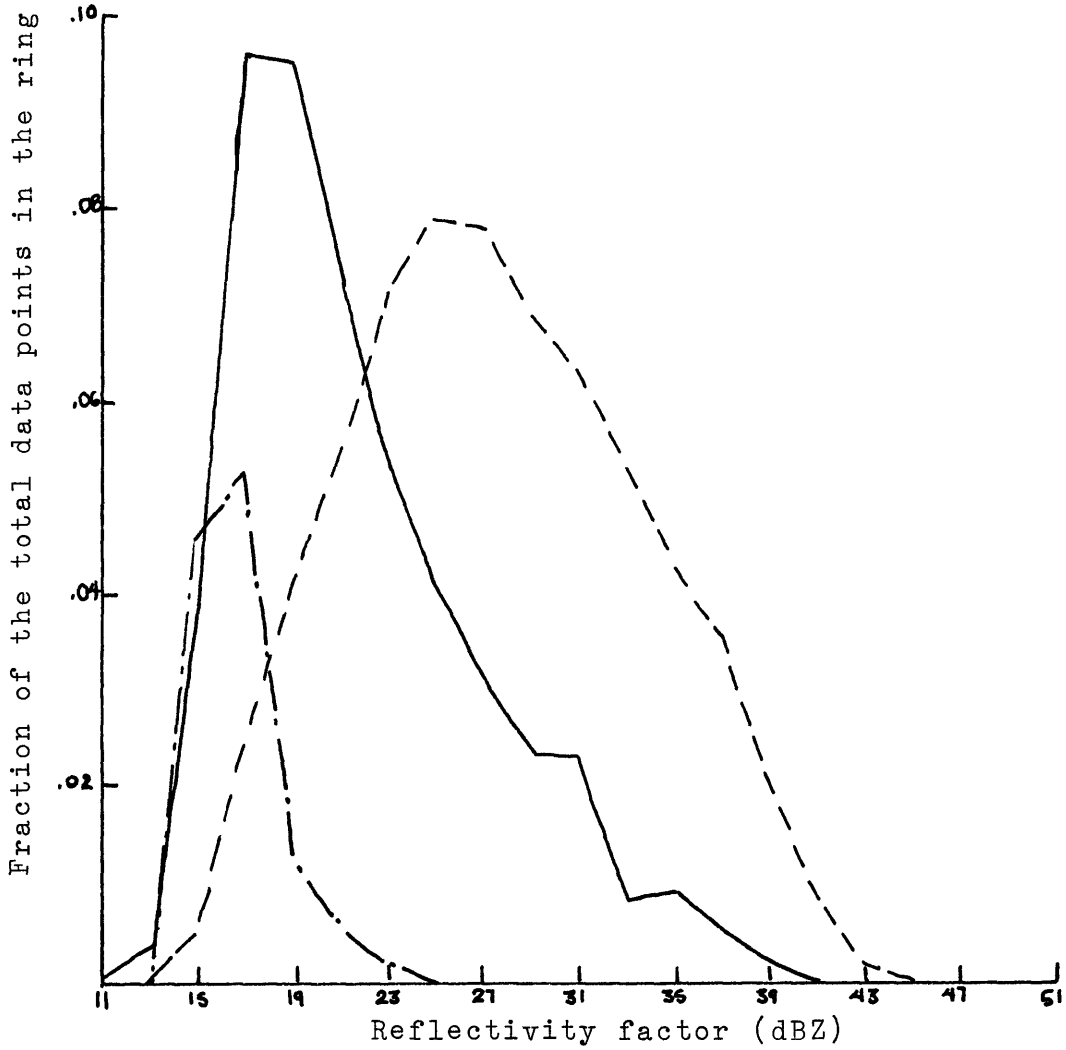


Figure 24. April 1, 1976, Ring 3.

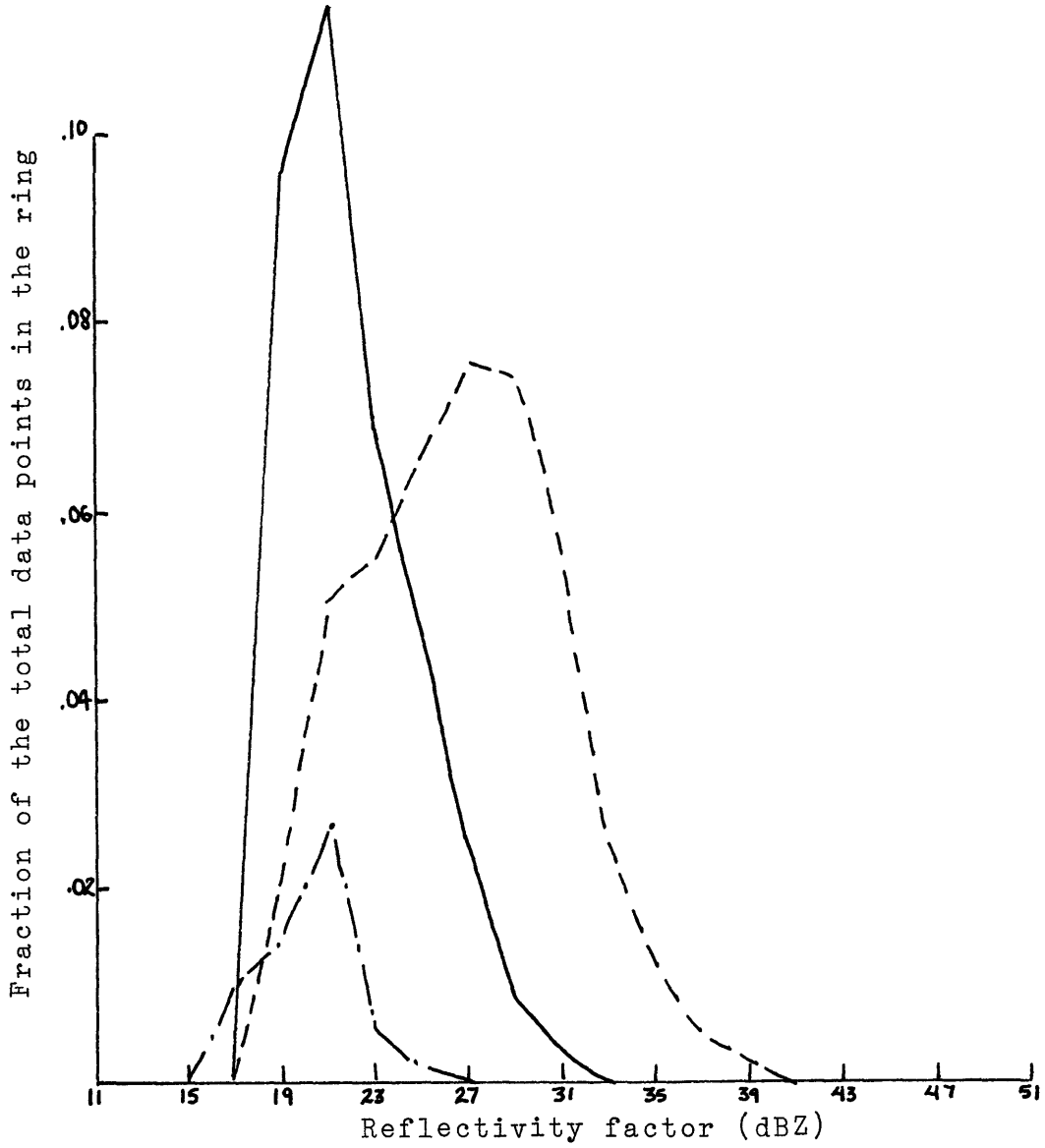


Figure 25. April 1, 1976, Ring 4.

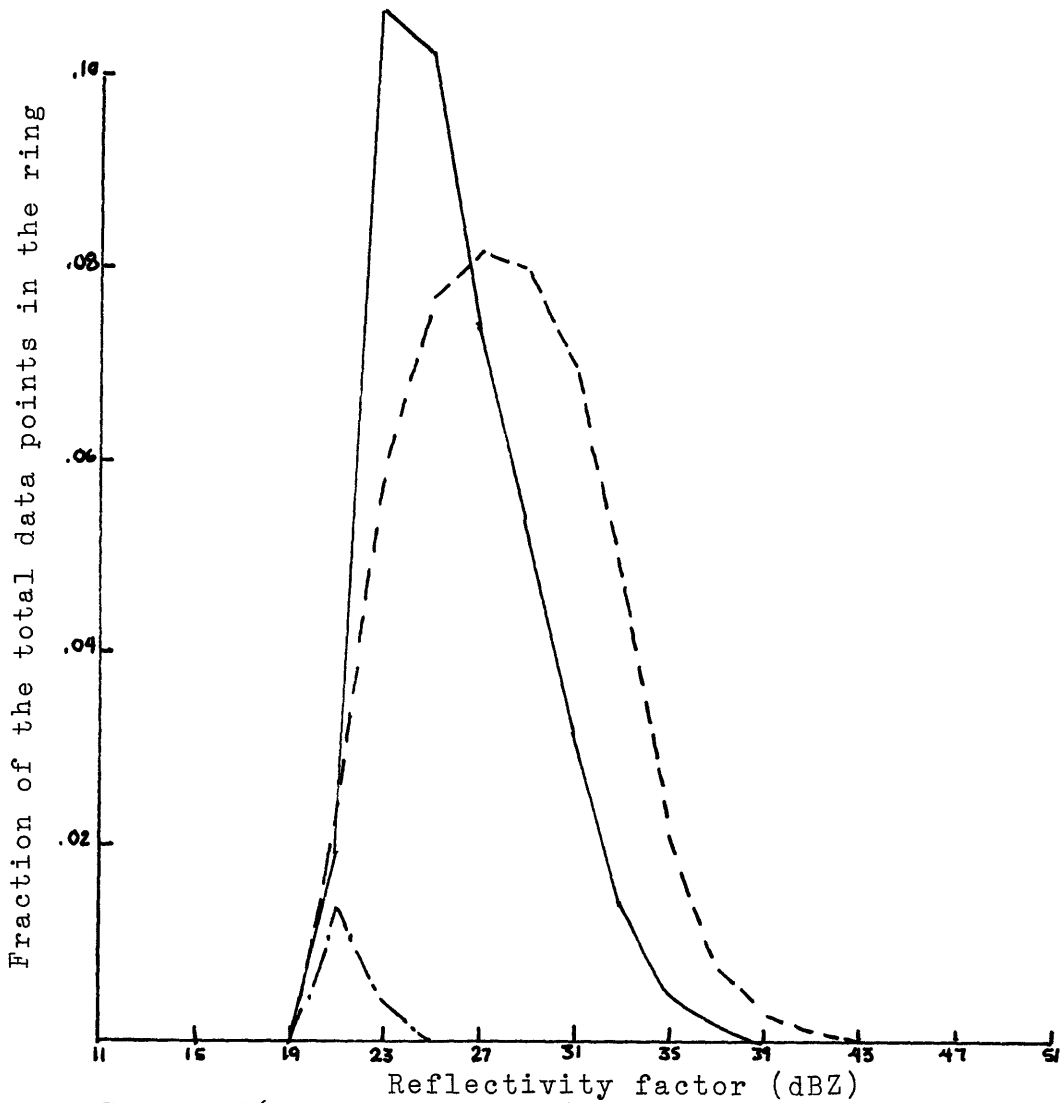


Figure 26. April 1, 1976, Ring 5.

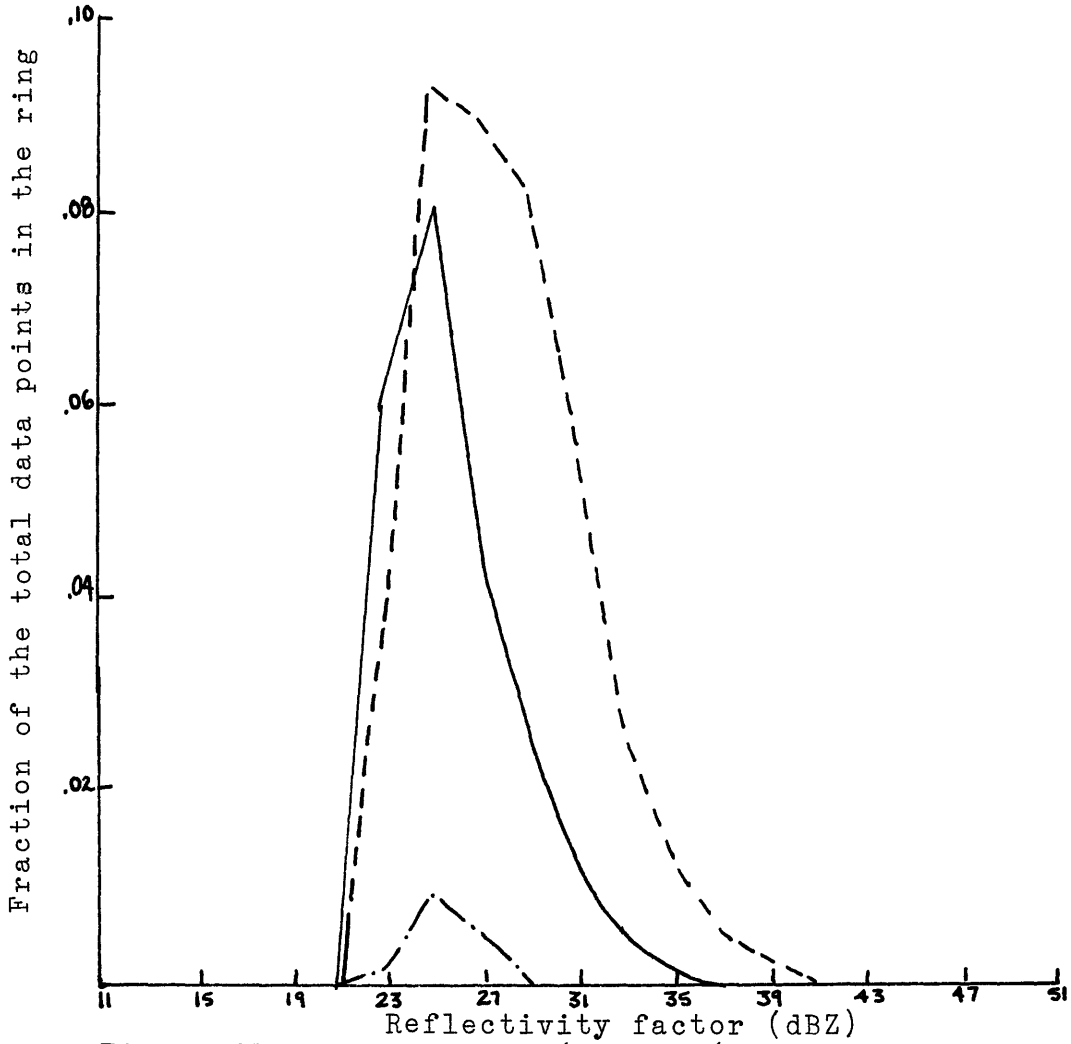


Figure 27. April 1, 1976, Ring 6.

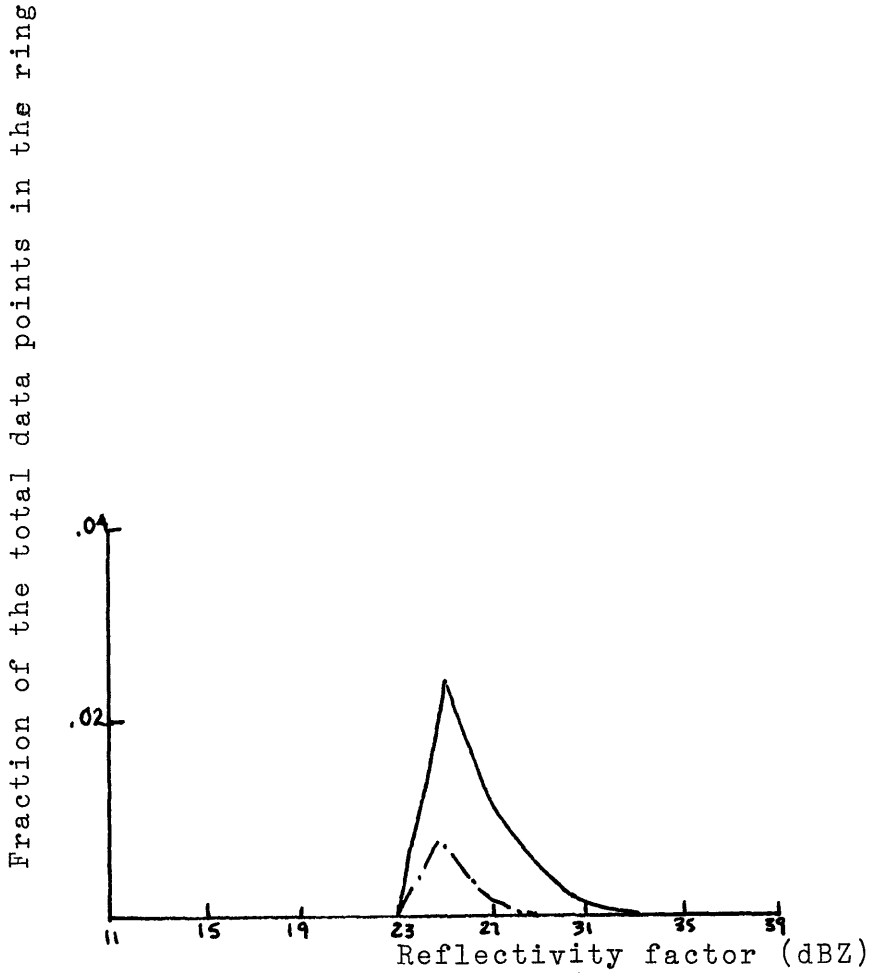


Figure 28. April 1, 1976, Ring 7.

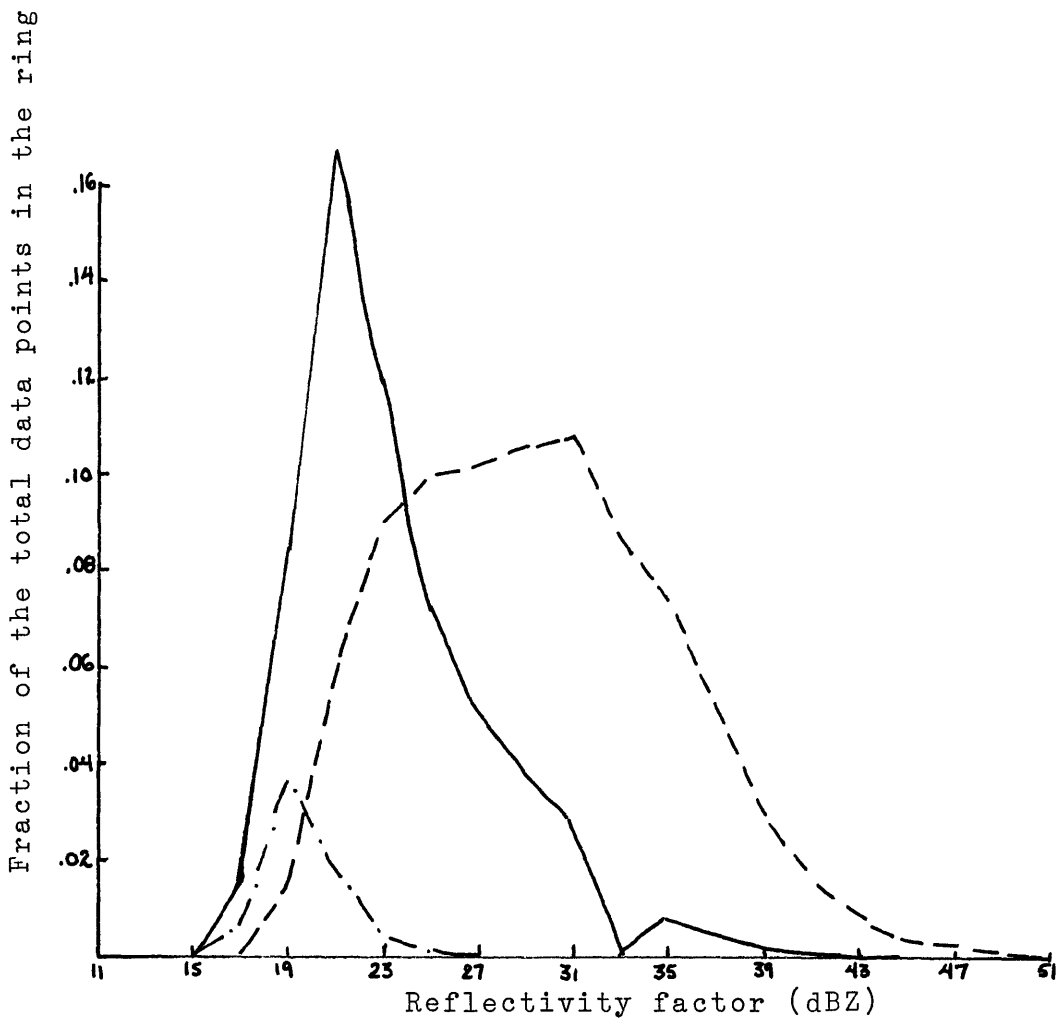


Figure 29. December 7, 1976, Ring 3.

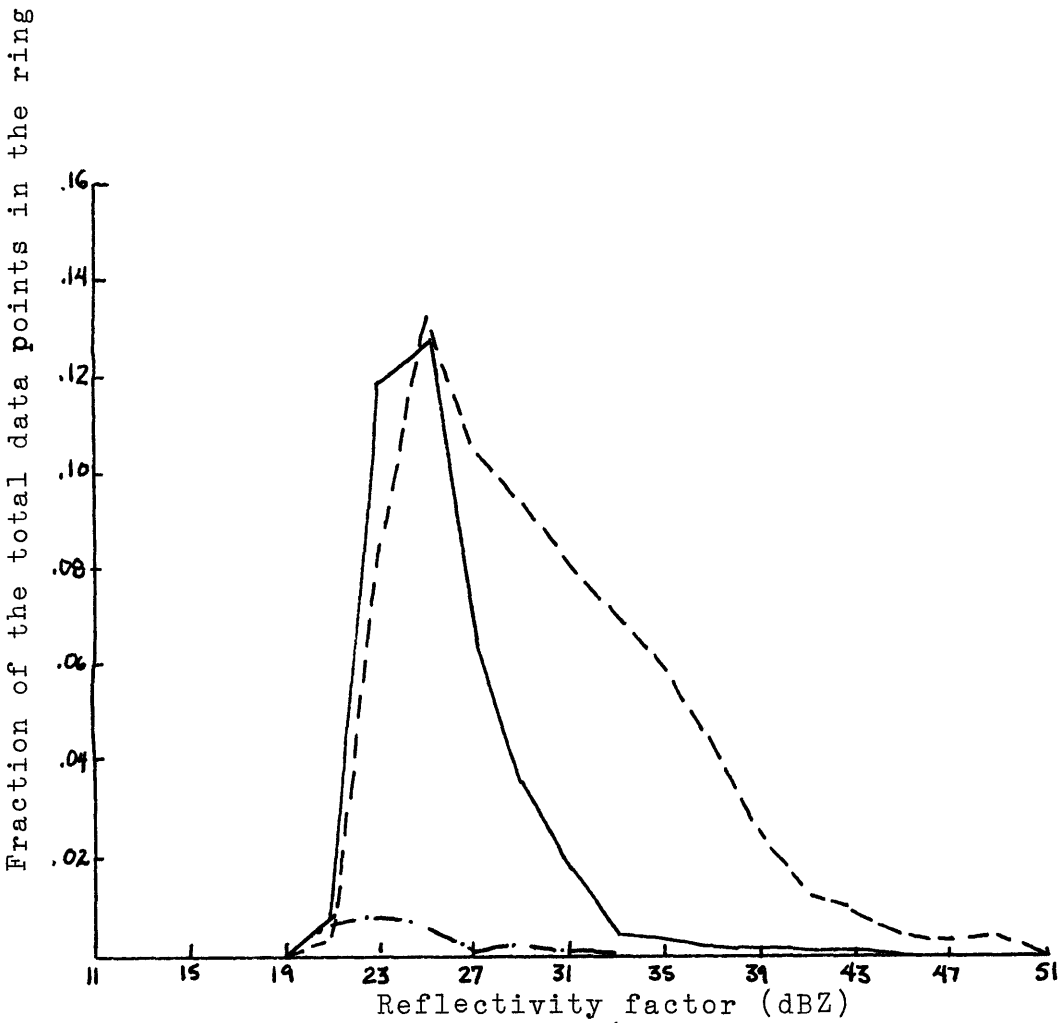


Figure 30. December 7, 1976, Ring 4.

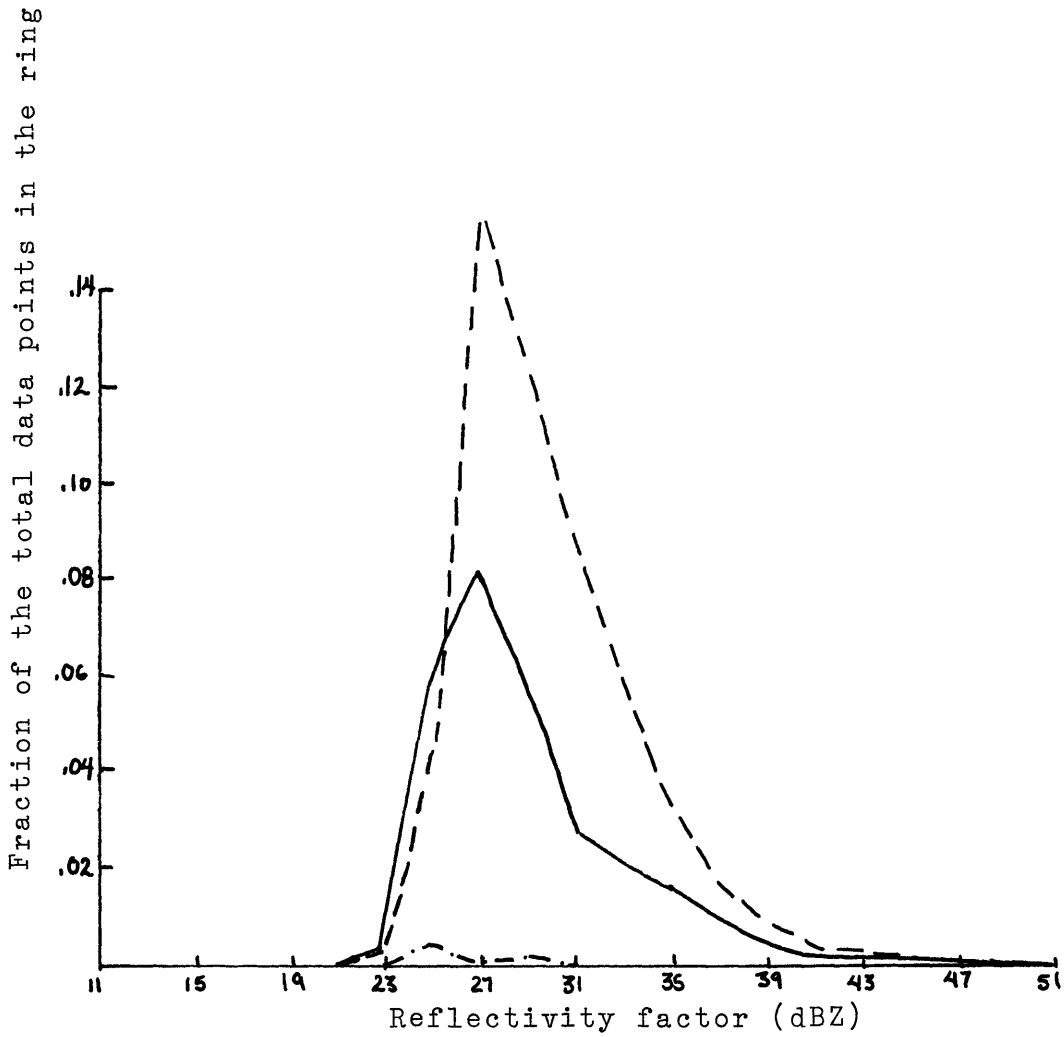


Figure 31. December 7, 1976, Ring 5.

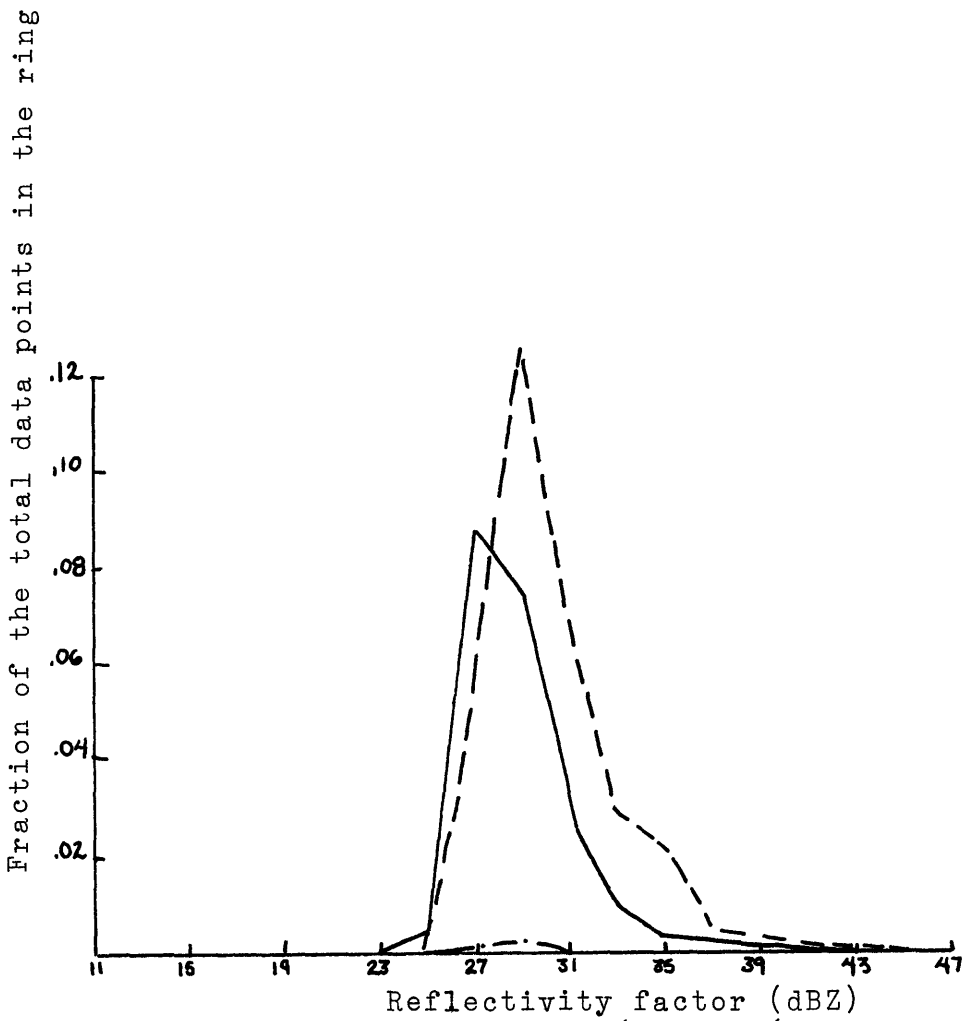


Figure 32. December 7, 1976, Ring 6.

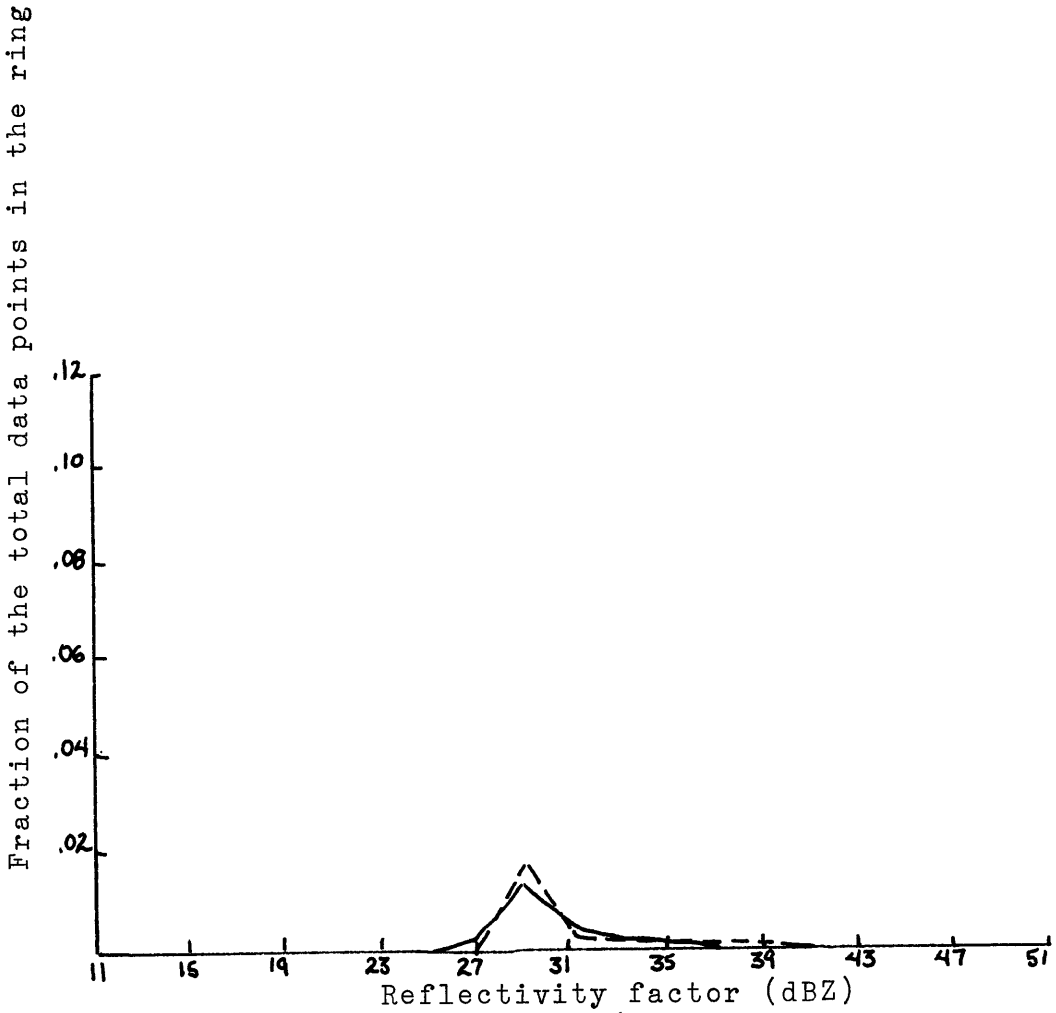


Figure 33. December 7, 1976, Ring 7.

# Appendix I

MAP NUMBER: 5065 12/ 7/1976 17: 14 HEIGHT = 6 0 KM.
THE NOMINAL ELEVATION ANGLES X 10 ARE: 5 10 20 30 40 60
THIS TABLE INCLUDES ATTENUATION

| DBZ VALUE < OR = TO | RING 1 | RING 2 | RING 3 | RING 4 | RING 5 | RING 6 | RING 7 | RING 8 |
|---|---|---|---|---|---|---|---|---|
| 0 | 0 | 4266 | 12050 | 10160 | 11265 | 1440 | 10231 | 14760 |
| 11 | 0 | 0 | 0 | 0 | 0 | 0 | 0 | 0 |
| 13 | 0 | 0 | 0 | 0 | 0 | 0 | 0 | 0 |
| 15 | 0 | 515 | 0 | 0 | 0 | 0 | 0 | 0 |
| 17 | 0 | 1027 | 133 | 0 | 0 | 0 | 0 | 0 |
| 19 | 0 | 225 | 829 | 0 | 0 | 0 | 0 | 0 |
| 21 | 0 | 70 | 605 | 154 | 0 | 0 | 0 | 0 |
| 23 | 0 | 0 | 60 | 111 | 36 | 0 | 0 | 0 |
| 25 | 0 | 0 | 0 | 203 | 100 | 0 | 0 | 0 |
| 27 | 0 | 0 | 0 | 39 | 69 | 0 | 60 | 0 |
| 29 | 0 | 0 | 0 | 28 | 37 | 0 | 124 | 0 |
| 31 | 0 | 0 | 0 | 22 | 4 | 0 | 12 | 0 |
| 33 | 0 | 0 | 0 | 12 | 0 | 0 | 7 | 0 |
| 35 | 0 | 0 | 0 | 20 | 4 | 0 | 4 | 0 |
| 37 | 0 | 0 | 0 | 22 | 5 | 0 | 2 | 0 |
| 39 | 0 | 0 | 0 | 17 | 0 | 0 | 0 | 0 |
| 41 | 0 | 0 | 0 | 9 | 0 | 0 | 0 | 0 |
| 43 | 0 | 0 | 0 | 2 | 0 | 0 | 0 | 0 |
| 45 | 0 | 0 | 0 | 1 | 0 | 0 | 0 | 0 |
| 47 | 0 | 0 | 0 | 0 | 0 | 0 | 0 | 0 |
| 49 | 0 | 0 | 0 | 0 | 0 | 0 | 0 | 0 |
| 51 | 0 | 0 | 0 | 0 | 0 | 0 | 0 | 0 |
| 53 | 0 | 0 | 0 | 0 | 0 | 0 | 0 | 0 |
| 55 | 0 | 0 | 0 | 0 | 0 | 0 | 0 | 0 |
| 57 | 0 | 0 | 0 | 0 | 0 | 0 | 0 | 0 |
| 59 | 0 | 0 | 0 | 0 | 0 | 0 | 0 | 0 |
| 61 | 0 | 0 | 0 | 0 | 0 | 0 | 0 | 0 |

# Appendix I (continued)

THIS IS A TABLE WHICH GIVES THE PERCENTAGE OF INDIVIDUAL DBZ INTENSITIES IN THE GIVEN RANGE RING

| DBZ VALUE < OR = TO | RING 1 | RING 2 | RING 3 | RING 4 | RING 5 | RING 6 | RING 7 | RING 8 |
|---|---|---|---|---|---|---|---|---|
| 0 | 0.000000 | 0.699000 | 0.881041 | 0.940741 | 0.977865 | 1.000000 | 0 979981 | 1.000000 |
| 11 | 0.000000 | 0.000000 | 0.000000 | 0.000000 | 0.000000 | 0.000000 | 0.000000 | 0 000000 |
| 13 | 0.000000 | 0.000000 | 0 000000 | 0 000000 | 0.000000 | 0.000000 | 0 000000 | 0.000000 |
| 15 | 0.000000 | 0 084385 | 0.000000 | 0 000000 | 0.000000 | 0.000000 | 0 000000 | 0.000000 |
| 17 | 0.000000 | 0.168278 | 0 009724 | 0.000000 | 0 000000 | 0 000000 | 0.000000 | 0.000000 |
| 19 | 0.000000 | 0 036867 | 0.060613 | 0 000000 | 0.000000 | 0 000000 | 0 000000 | 0.000000 |
| 21 | 0.000000 | 0.011470 | 0 044235 | 0 014259 | 0 000000 | 0.000000 | 0 000000 | 0.000000 |
| 23 | 0.000000 | 0.000000 | 0 004387 | 0 010278 | 0.003125 | 0.000000 | 0 000000 | 0.000000 |
| 25 | 0.000000 | 0 000000 | 0 000000 | 0 018796 | 0 008681 | 0 000000 | 0.000000 | 0.000000 |
| 27 | 0.000000 | 0.000000 | 0.000000 | 0.003611 | 0.005990 | 0 000000 | 0 005747 | 0.000000 |
| 29 | 0.000000 | 0.000000 | 0 000000 | 0.002593 | 0 003212 | 0.000000 | 0.011877 | 0.000000 |
| 31 | 0.000000 | 0.000000 | 0.000000 | 0.002037 | 0 000347 | 0 000000 | 0.001149 | 0.000000 |
| 33 | 0.000000 | 0.000000 | 0 000000 | 0.001111 | 0 000000 | 0.000000 | 0.000670 | 0.000000 |
| 35 | 0 000000 | 0.000000 | 0 000000 | 0 001852 | 0.000347 | 0 000000 | 0.000383 | 0 000000 |
| 37 | 0.000000 | 0 000000 | 0 000000 | 0 002037 | 0 000434 | 0.000000 | 0 000192 | 0.000000 |
| 39 | 0 000000 | 0 000000 | 0 000000 | 0 001574 | 0 000000 | 0.000000 | 0.000000 | 0 000000 |
| 41 | 0.000000 | 0 000000 | 0 000000 | 0 000833 | 0 000000 | 0.000000 | 0 000000 | 0.000000 |
| 43 | 0.000000 | 0 000000 | 0.000000 | 0 000185 | 0 000000 | 0 000000 | 0 000000 | 0.000000 |
| 45 | 0 000000 | 0.000000 | 0.000000 | 0 000093 | 0 000000 | 0.000000 | 0 000000 | 0.000000 |
| 47 | 0.000000 | 0.000000 | 0 000000 | 0 000000 | 0 000000 | 0.000000 | 0 000000 | 0.000000 |
| 49 | 0.000000 | 0 000000 | 0.000000 | 0.000000 | 0.000000 | 0.000000 | 0 000000 | 0.000000 |
| 51 | 0 000000 | 0.000000 | 0.000000 | 0.000000 | 0.000000 | 0.000000 | 0.000000 | 0.000000 |
| 53 | 0 000000 | 0 000000 | 0 000000 | 0 000000 | 0 000000 | 0 000000 | 0.000000 | 0.000000 |
| 55 | 0.000000 | 0 000000 | 0.000000 | 0 000000 | 0 000000 | 0.000000 | 0 000000 | 0.000000 |
| 57 | 0 000000 | 0 000000 | 0 000000 | 0 000000 | 0 000000 | 0.000000 | 0 000000 | 0.000000 |
| 59 | 0.000000 | 0 000000 | 0.000000 | 0 000000 | 0 000000 | 0.000000 | 0 000000 | 0 000000 |
| 61 | 0.000000 | 0 000000 | 0 000000 | 0 000000 | 0 000000 | 0 000000 | 0 000000 | 0.000000 |

THE FOLLOWING ARE THE NUMBER OF BINS CONTAINED IN EACH RANGE RING

| | | | | | | | |
|---|---|---|---|---|---|---|---|
| 0 | 6103 | 13677 | 10800. | 11520. | 1440 | 10440 | 14760. |

## Appendix II

### Summary of the number of points in each range ring

### April 1, 1976

| Time: | Hgt.(km) | Ring 1 | Ring 2 | Ring 3 | Ring 4 | Ring 5 | Ring 6 | Ring 7 | Ring 8 |
|---|---|---|---|---|---|---|---|---|---|
| 11:31 | 2 | 12942 | 24829 | 24480 | 23040 | 17640 | 1440 | 0 | 0 |
| | 4 | 0 | 11138 | 17275 | 10080 | 5760 | 21960 | 16569 | 1080 |
| | 6 | 0 | 0 | 12573 | 10800 | 11520 | 1440 | 6840 | 22320 |
| 12:01 | 2 | 12942 | 24829 | 24480 | 23040 | 17640 | 1440 | 0 | 0 |
| | 4 | 0 | 11138 | 17275 | 10080 | 5760 | 21960 | 16560 | 1080 |
| | 6 | 0 | 0 | 12573 | 10800 | 11520 | 1440 | 6840 | 22320 |
| 12:46 | 2 | 13662 | 26629 | 23400 | 23040 | 14400 | 1440 | 0 | 0 |
| | 4 | 0 | 11138 | 18355 | 8280 | 9000 | 21960 | 12960 | 1080 |
| | 6 | 0 | 0 | 12573 | 12600 | 10800 | 0 | 10440 | 18720 |
| 13:30 | 2 | 13662 | 26629 | 23400 | 23040 | 14400 | 1440 | 0 | 0 |
| | 4 | 0 | 11138 | 18355 | 8280 | 9000 | 21960 | 12960 | 1080 |
| | 6 | 0 | 0 | 12573 | 12600 | 10800 | 0 | 10440 | 18720 |
| 13:45 | 2 | 14021 | 26270 | 23400 | 23040 | 14400 | 1440 | 0 | 0 |
| | 4 | 0 | 11497 | 17996 | 8280 | 9000 | 21960 | 12960 | 1080 |
| | 6 | 0 | 0 | 12214 | 12600 | 10800 | 0 | 10440 | 18720 |
| 14:15 | 2 | 12942 | 26629 | 24480 | 23040 | 14400 | 1440 | 0 | 0 |
| | 4 | 0 | 11138 | 17275 | 10080 | 9000 | 21960 | 12960 | 1080 |
| | 6 | 0 | 0 | 12573 | 10800 | 11520 | 1440 | 10440 | 18720 |
| 14:45 | 2 | 7186 | 24456 | 23400 | 23040 | 11880 | 1440 | 0 | 0 |
| | 4 | 0 | 3231 | 16535 | 8280 | 11520 | 20160 | 11520 | 1080 |
| | 6 | 0 | 0 | 2872 | 12575 | 10800 | 2160 | 11520 | 15120 |

### September 24, 1975

| Time: | Hgt.(km) | Ring 1 | Ring 2 | Ring 3 | Ring 4 | Ring 5 | Ring 6 | Ring 7 | Ring 8 |
|---|---|---|---|---|---|---|---|---|---|
| 14:30 | 2 | 31308 | 29880 | 26280 | 18360 | 6120 | 0 | 0 | 0 |
| | 4 | 10429 | 19080 | 17280 | 11880 | 17280 | 15480 | 5040 | 0 |
| | 6 | 1795 | 14393 | 12960 | 12960 | 9000 | 7920 | 16200 | 11520 |
| 14:57 | 2 | 31308 | 29880 | 26280 | 18360 | 6120 | 0 | 0 | 0 |
| | 4 | 10428 | 19080 | 17280 | 11880 | 17280 | 15480 | 5040 | 0 |
| | 6 | 1795 | 14034 | 12960 | 12960 | 9000 | 7920 | 16200 | 11520 |
| 16:17 | 2 | 30948 | 30240 | 26280 | 18360 | 6120 | 0 | 0 | 0 |
| | 4 | 10428 | 18720 | 17640 | 11880 | 17280 | 15480 | 5040 | 0 |
| | 6 | 1795 | 14393 | 13320 | 12960 | 9000 | 7920 | 16200 | 11520 |
| 16:56 | 2 | 31308 | 29880 | 26280 | 18360 | 6120 | 0 | 0 | 0 |
| | 4 | 10428 | 19080 | 17280 | 11880 | 17280 | 15480 | 5040 | 0 |
| | 6 | 1795 | 14393 | 12960 | 12960 | 9000 | 7920 | 16200 | 11520 |

Appendix II (continued)

December 7, 1976

| Time: | Hgt.(km) | Ring 1 | Ring 2 | Ring 3 | Ring 4 | Ring 5 | Ring 6 | Ring 7 | Ring 8 |
|---|---|---|---|---|---|---|---|---|---|
| 12:17 | 2 | 17978 | 27720 | 16920 | 20520 | 23040 | 12960 | 2160 | 0 |
| | 4 | 718 | 14381 | 17640 | 13320 | 3960 | 10440 | 21240 | 12600 |
| | 6 | 0 | 5026 | 10434 | 12240 | 10800 | 7560 | 0 | 20670 |
| 13:16 | 2 | 17978 | 27720 | 18360 | 23040 | 23040 | 10800 | 0 | 0 |
| | 4 | 718 | 14381 | 17640 | 13320 | 3960 | 12960 | 23040 | 10440 |
| | 6 | 0 | 5026 | 10434 | 12240 | 10800 | 7560 | 0 | 13320 |
| 14:15 | 2 | 17619 | 27720 | 16920 | 20520 | 23040 | 12960 | 2160 | 0 |
| | 4 | 1077 | 14022 | 17640 | 13320 | 3960 | 10440 | 21240 | 12600 |
| | 6 | 0 | 5385 | 10075 | 12240 | 10800 | 7560 | 0 | 20670 |
| 15:21 | 2 | 30228 | 28440 | 21600 | 23040 | 11880 | 5040 | 0 | 0 |
| | 4 | 10067 | 18360 | 17280 | 10080 | 11520 | 16560 | 11520 | 5040 |
| | 6 | 1436 | 14392 | 13680 | 10800 | 11520 | 3600 | 11520 | 11160 |
| 16:12 | 2 | 20140 | 26640 | 21600 | 23040 | 14400 | 5040 | 0 | 0 |
| | 4 | 1436 | 16904 | 17280 | 10080 | 9000 | 18360 | 12960 | 5040 |
| | 6 | 0 | 6103 | 13677 | 10800 | 11520 | 1440 | 10440 | 14760 |
| 17:14 | 2 | 20140 | 26640 | 21600 | 23040 | 14400 | 5040 | 0 | 0 |
| | 4 | 1436 | 16904 | 17280 | 10080 | 9000 | 18360 | 12960 | 5040 |
| | 6 | 0 | 6103 | 13677 | 10800 | 11520 | 1440 | 10440 | 14760 |

August 13, 1976

| Time: | Hgt.(km) | Ring 1 | Ring 2 | Ring 3 | Ring 4 | Ring 5 | Ring 6 | Ring 7 | Ring 8 |
|---|---|---|---|---|---|---|---|---|---|
| 18:14 | 2 | 25904 | 27000 | 27000 | 23040 | 12240 | 0 | 0 | 0 |
| | 4 | 5389 | 17996 | 18000 | 10080 | 11520 | 23040 | 10080 | 0 |
| | 6 | 0 | 11505 | 13320 | 11160 | 11520 | 1440 | 13680 | 19440 |
| 18:50 | 2 | 30948 | 25200 | 25920 | 23040 | 15480 | 0 | 0 | 0 |
| | 4 | 9708 | 18000 | 19080 | 8280 | 8280 | 23040 | 13680 | 0 |
| | 6 | 1795 | 14033 | 13320 | 12960 | 10800 | 0 | 10080 | 23040 |
| 19:29 | 2 | | 25920 | 27360 | 23040 | 12240 | 0 | 0 | 0 |
| | 4 | 16552 | 18000 | 19080 | 8280 | 11520 | 23040 | 10080 | 0 |
| | 6 | 8271 | 14400 | 13320 | 12960 | 10800 | 0 | 13680 | 23040 |
| 19:49 | 2 | 29868 | 26280 | 28440 | 23040 | 12240 | 0 | 0 | 0 |
| | 4 | 9708 | 17640 | 19080 | 10080 | 11520 | 23040 | 10080 | 0 |
| | 6 | 1795 | 14392 | 12240 | 12600 | 11520 | 1440 | 13680 | 23040 |
| 20:18 | 2 | | 25920 | 28440 | 23040 | 12240 | 0 | 0 | 0 |
| | 4 | 19073 | 18000 | 18000 | 10080 | 11520 | 23040 | 10080 | 0 |
| | 6 | 10434 | 14400 | 13320 | 11160 | 11520 | 1440 | 13680 | 23040 |

Note: Blanks indicate bad data.

# Appendix III

## Storm summaries for April 1, 1976

HEIGHT = 2.0

| DBZ VALUE < OR = TO | RING 1 | RING 2 | RING 3 | RING 4 | RING 5 | RING 6 | RING 7 | RING 8 |
|---|---|---|---|---|---|---|---|---|
| 0 | 55264. | 64118. | 62113. | 71624. | 55406. | 6012. | 0. | 0. |
| 11 | 1471. | 2336. | 0. | 0. | 0. | 0. | 0. | 0. |
| 13 | 1679. | 3362. | 0. | 0. | 0. | 0. | 0. | 0. |
| 15 | 2001. | 5473. | 774. | 0. | 0. | 0. | 0. | 0. |
| 17 | 2203. | 6573. | 4259. | 0. | 0. | 0. | 0. | 0. |
| 19 | 2672 | 8580 | 6851. | 3178. | 0. | 0. | 0. | 0. |
| 21 | 2840. | 10646. | 8975. | 8152. | 2464. | 0. | 0. | 0. |
| 23 | 2858. | 12151. | 11831. | 8831. | 6232. | 410. | 0. | 0. |
| 25 | 3760. | 12091. | 13115. | 10629. | 8047. | 936. | 0. | 0. |
| 27 | 4164. | 13035. | 12999. | 12195. | 8628. | 899. | 0. | 0. |
| 29 | 4248. | 13659. | 11497. | 11887. | 8408 | 822. | 0. | 0. |
| 31 | 3060. | 12099 | 10552. | 9985. | 7290. | 559. | 0. | 0. |
| 33 | 908 | 6827. | 6189. | 9097. | 4920. | 251. | 0. | 0. |
| 35 | 163. | 4894. | 7112. | 8045 | 2246. | 124. | 0. | 0. |
| 37 | 52. | 2565. | 5875. | 4751. | 760 | 49. | 0. | 0. |
| 39 | 14. | 1211. | 3391. | 2097. | 275. | 18. | 0. | 0. |
| 41 | 0. | 530. | 1267. | 702. | 64. | 0. | 0. | 0. |
| 43 | 0. | 115. | 215. | 107. | 14. | 0. | 0. | 0. |
| 45 | 0. | 6. | 25. | 0. | 6. | 0. | 0. | 0. |
| 47 | 0. | 0. | 0. | 0. | 0. | 0. | 0. | 0. |
| 49 | 0. | 0. | 0. | 0. | 0. | 0. | 0. | 0. |
| 51 | 0. | 0. | 0. | 0. | 0. | 0. | 0. | 0. |
| 53 | 0. | 0. | 0. | 0. | 0. | 0. | 0. | 0. |
| 55 | 0. | 0. | 0. | 0. | 0 | 0. | 0. | 0. |
| 57 | 0. | 0. | 0. | 0. | 0. | 0. | 0. | 0. |
| 59 | 0. | 0. | 0. | 0. | 0. | 0. | 0. | 0. |
| 61 | 0. | 0. | 0. | 0. | 0. | 0. | 0. | 0. |

## Appendix III (continued)

HEIGHT = 4.0

| DBZ VALUE < OR = TO | RING 1 | RING 2 | RING 3 | RING 4 | RING 5 | RING 6 | RING 7 | RING 8 |
|---|---|---|---|---|---|---|---|---|
| 0 | 0. | 28826. | 61243. | 40319. | 34807. | 117033. | 92499. | 7560. |
| 11 | 0. | 464. | 0. | 0. | 0. | 0. | 0. | 0. |
| 13 | 0 | 3976. | 350. | 0. | 0. | 0. | 0. | 0. |
| 15 | 0. | 6435. | 4982. | 0. | 0. | 0. | 0. | 0. |
| 17 | 0 | 6644. | 11849. | 0. | 0. | 0. | 0. | 0. |
| 19 | 0 | 5985. | 11741. | 6055. | 0. | 0. | 0. | 0. |
| 21 | 0 | 4458. | 8813. | 7250 | 1209. | 0. | 0. | 0. |
| 23 | 0. | 3734. | 6760. | 4375. | 6323 | 9112. | 0 | 0. |
| 25 | 0 | 3355 | 5041 | 2965. | 6060 | 12290. | 2353. | 0. |
| 27 | 0. | 2446. | 3759 | 1670. | 4381. | 6483. | 1027. | 0. |
| 29 | 0. | 1877. | 2832. | 545. | 3174. | 3917. | 409. | 0. |
| 31 | 0. | 1192. | 2872. | 173. | 1906. | 2016. | 142. | 0. |
| 33 | 0. | 681 | 923. | 6. | 848. | 804. | 45. | 0. |
| 35 | 0. | 262. | 1089. | 2. | 266. | 215. | 5. | 0. |
| 37 | 0. | 70 | 585. | 0. | 52. | 50. | 0. | 0. |
| 39 | 0. | 13. | 193. | 0. | 12. | 0. | 0. | 0. |
| 41 | 0. | 0. | 33. | 0. | 2. | 0. | 0. | 0. |
| 43 | 0. | 0. | 1. | 0. | 0. | 0. | 0. | 0. |
| 45 | 0. | 0. | 0. | 0. | 0. | 0. | 0. | 0. |
| 47 | 0. | 0. | 0. | 0. | 0. | 0. | 0. | 0. |
| 49 | 0. | 0. | 0. | 0. | 0. | 0. | 0. | 0. |
| 51 | 0. | 0. | 0. | 0. | 0. | 0. | 0. | 0. |
| 53 | 0. | 0. | 0. | 0. | 0. | 0. | 0. | 0. |
| 55 | 0. | 0. | 0. | 0. | 0. | 0. | 0. | 0. |
| 57 | 0. | 0. | 0. | 0. | 0. | 0. | 0. | 0. |
| 59 | 0. | 0. | 0. | 0. | 0 | 0 | 0. | 0. |
| 61 | 0. | 0. | 0. | 0. | 0. | 0. | 0. | 0. |

## Appendix III (continued)

HEIGHT = 6.0

| DBZ VALUE < OR = TO | RING 1 | RING 2 | RING 3 | RING 4 | RING 5 | RING 6 | RING 7 | RING 8 |
|---|---|---|---|---|---|---|---|---|
| 0 | 0. | 0. | 68561. | 78043. | 76295. | 6374. | 66280. | 134640. |
| 11 | 0. | 0. | 0. | 0. | 0. | 0. | 0. | 0. |
| 13 | 0. | 0. | 0. | 0. | 0. | 0. | 0. | 0. |
| 15 | 0. | 0. | 3615. | 0. | 0. | 0. | 0. | 0. |
| 17 | 0. | 0. | 4167. | 816. | 0. | 0. | 0. | 0. |
| 19 | 0. | 0. | 1032. | 1240. | 0. | 0. | 0. | 0. |
| 21 | 0. | 0. | 453. | 2232. | 1121. | 0. | 0. | 0. |
| 23 | 0. | 0 | 121. | 392. | 314. | 10. | 0. | 0. |
| 25 | 0. | 0. | 2. | 43. | 26. | 60. | 542. | 0. |
| 27 | 0. | 0. | 0. | 5. | 4. | 33. | 127. | 0. |
| 29 | 0. | 0. | 0. | 3. | 0. | 3. | 11. | 0. |
| 31 | 0. | 0. | 0. | 0. | 0. | 0. | 0. | 0. |
| 33 | 0. | 0. | 0. | 0. | 0 | 0. | 0. | 0. |
| 35 | 0. | 0. | 0. | 1. | 0. | 0. | 0. | 0. |
| 37 | 0. | 0. | 0. | 0. | 0. | 0. | 0. | 0. |
| 39 | 0. | 0. | 0. | 0. | 0. | 0. | 0. | 0. |
| 41 | 0. | 0. | 0. | 0. | 0. | 0. | 0. | 0. |
| 43 | 0. | 0. | 0. | 0. | 0. | 0. | 0. | 0. |
| 45 | 0. | 0. | 0. | 0. | 0. | 0. | 0. | 0. |
| 47 | 0. | 0. | 0. | 0. | 0. | 0. | 0. | 0. |
| 49 | 0. | 0. | 0. | 0. | 0. | 0. | 0. | 0. |
| 51 | 0. | 0. | 0. | 0. | 0. | 0. | 0. | 0. |
| 53 | 0. | 0. | 0. | 0. | 0 | 0. | 0. | 0. |
| 55 | 0. | 0. | 0. | 0. | 0. | 0. | 0. | 0. |
| 57 | 0. | 0. | 0. | 0. | 0. | 0. | 0. | 0. |
| 59 | 0. | 0. | 0. | 0. | 0. | 0. | 0. | 0. |
| 61 | 0. | 0. | 0. | 0. | 0. | 0. | 0. | 0. |

## References

Battan, L.J. (1973): Radar Observations of the Atmosphere. University of Chicago Press, 324 pp.

Geotis, S.G. (1975): Some measurements of the attenuation of 5-cm. radiation in rain. 16th Radar Meteorology Conference Preprints, American Meteorological Society, Boston, pp. 63-66.

Gunn, K.L.S. and T.W.R. East (1954): The microwave properties of precipitation particles. Quarterly Journal of the Royal Meteorological Society, vol. 80, pp. 522-545.

Skolnik, M.I. (1970): Radar Handbook. McGraw-Hill Book Company.

Smithsonian Meteorological Tables (1951) Smithsonian Miscellaneous Collections, Smithsonian Institution, Washington, D.C.

U.S. Standard Atmosphere Supplements, 1966. Prepared under the sponsorship of Environmental Science Services Administration, National Aeronautics and Space Administration, and the United States Air Force. For sale by the Superintendent of Documents, U.S. Government Printing Office.